Hole spin relaxation in bilayer WSe_2

F. Yang,[1] L. Wang,[1] and M. W. Wu[1,2,*]

[1]*Hefei National Laboratory for Physical Sciences at Microscale and Department of Physics, University of Science and Technology of China, Hefei, Anhui, 230026, China*
[2]*Department of Physics, Kyushu University, 6-10-1 Hakozaki, Fukuoka, 812-8581, Japan*

(Dated: June 16, 2015)

We investigate the hole spin relaxation due to the Rashba spin-orbit coupling induced by an external perpendicular electric field in bilayer WSe_2. The Rashba spin-orbit coupling coefficients in bilayer WSe_2 are constructed from the corresponding monolayer ones. In contrast to monolayer WSe_2, the out-of-plane component of the bilayer Rashba spin-orbit coupling acts as a Zeeman-like field with opposite directions but identical values in the two valleys. For in-plane spins, this Zeeman-like field, together with the intervalley hole-phonon scattering, opens an intervalley spin relaxation channel, which is found to dominate the in-plane spin relaxation in bilayer WSe_2 even at low temperature. For out-of-plane spins, this Zeeman-like field is superimposed by the identical Hartree-Fock effective magnetic fields in the two valleys, and hence different total effective magnetic fields between two valleys are obtained. Owing to the large difference of the total fields at large spin polarization, different out-of-plane spin relaxation times in the two valleys are obtained when the intervalley hole-phonon scattering is weak at low temperature and low hole density. This difference in the spin relaxation times can be suppressed by enhancing the intervalley hole-phonon scattering through increasing temperature or hole density. Moreover, at large spin polarization and low temperature, due to the weak intravalley hole-phonon scattering but relatively strong hole-hole Coulomb scattering, the fast spin precessions are found to result in a quasi hot-hole Fermi distribution characterized by an effective hot-hole temperature larger than the temperature, which also enhances the intervalley scattering. During this process, it is interesting to discover that the initially equal hole densities in the two valleys are broken in the temporal evolution, and a valley polarization is built up. It is further revealed that this comes from the different spin relaxation processes at large spin polarization and different spin-conserving intervalley scattering rates between spin-up and -down holes due to the different effective hot-hole temperatures.

PACS numbers: 72.25.Rb, 71.10.w, 71.70.Ej, 72.10.Di

I. INTRODUCTION

Very recently, the spin dynamics in monolayer (ML) transition metal dichalcogenides (TMDs) has attracted much attention,[1–7] partly due to their unique electric[8–18] and novel optical[15,18–22] properties. Specifically, owing to the direct gap at the K (K′) point[8–11] and large energy spin splitting of the valence bands,[13,16,17] the chiral optical valley selection rule in ML TMDs[19–22] allows optical control of the valley pseudospin[23–27] and real spin,[11–16,19–22] making them promising candidates for the spintronic application.

Among these studies in ML TMDs, carrier spin relaxation due to the Elliot-Yafet[28,29] (EY) and D'yakonov-Perel'[30] (DP) mechanisms is an important property to understand for any possible spintronic applications. For the intrinsic EY mechanism, it was claimed that the intervalley out-of-plane spin-flip scattering is forbidden by the time reversal symmetry, while the flexural phonon vibrations thermally activated at high temperature can lead to the intravalley out-of-plane spin relaxation.[1] Additionally, due to the marginal in-plane spin mixing, the contribution of the EY mechanism to the in-plane spin relaxation is negligible.[5] For the DP mechanism, in the intrinsic situation, the out-of-plane spin relaxation processes are forbidden due the good quantum number of σ_z but the in-plane processes exist,[4,5] including the intravalley and intervalley processes. Particularly, the intervalley process arises from the intrinsic spin-orbit coupling (SOC), which acts as opposite effective magnetic fields in the two valleys and hence opens an intervalley in-plane spin relaxation channel in the presence of the intervalley carrier-phonon scatterings. The extrinsic influence such as the flexural deformations,[3] the external in-plane magnetic field,[5] or the Rashba SOC induced by an external perpendicular electric field,[2] can cause the out-of-plane spin relaxation. Moreover, in contrast to the electron spin relaxation, the hole spin relaxation processes are markedly suppressed due to the large energy splitting of the valence bands.[1–3]

Consisting of two-layer TMDs, bilayer (BL) TMDs also obey the chiral optical valley selection rule and possess good spin characters,[31–46] apart from new features such as layer pseudospin,[41] electrical-tuned magnetic moments[32] and magnetoelectric effect.[33] Specifically, due to the 180° in-plane rotation between the upper and lower layers in BL TMDs, in the K (K′) valley, the hole bands in one layer have opposite spin polarizations between the energy-degenerate ones in another layer. The interlayer hopping, which exists only in holes in the same valley with the same spin, has no influence on this spin degeneracy. This is very different from the ML TMDs, where the hole bands possessing opposite spin polarizations in the K (K′) valley are largely energy split,

markedly suppressing the hole spin relaxation. In BL TMDs, with the intrinsic EY hole spin relaxation and the intrinsic DP in-plane one suppressed in each layer while the intrinsic DP out-of-plane one forbidden, the Rashba SOC of the lowest two degenerate hole bands[33]

$$\mathbf{\Omega}^{\mu} = \big[-\nu(1+\alpha k^2)k_y, \nu(1+\alpha k^2)k_x, \mu\eta \big] E_z, \qquad (1)$$

induced by an external perpendicular electric field E_z, is expected to make the dominant contribution to the hole spin relaxation. Here, the $\hat{z}$-axis is set to be perpendicular to the BL TMD plane; $\mu = 1(-1)$ representing the K (K′) valley. The out-of-plane component of Rashba SOC serves as a Zeeman-like term $\mu\eta E_z$ with opposite effective magnetic fields in the two valleys.[33,35] Due to this coupling of real spin and valley pseudospin, one may expect the interplay of the spin polarization with the valley polarization and the rich physics of spin and valley dynamics in BL TMDs. Specifically, for in-plane spins, this Zeeman-like term, together with the intervalley hole-phonon scattering, opens a new intervalley spin relaxation channel. For out-of-plane spins, this Zeeman-like term is superimposed by the Coulomb Hartree-Fock (HF) self-energy, which has been understood first theoretically[47–49] and then experimentally[50] in semiconductors to serve as an effective magnetic field

$$\mathbf{\Omega}_{\rm HF}(\mathbf{k}) = -\sum_{\mathbf{k}'} V_{\mathbf{k}-\mathbf{k}'} {\rm Tr}\big[\rho_{\mathbf{k}'}\boldsymbol{\sigma}\big], \qquad (2)$$

with $V_{\mathbf{k}-\mathbf{k}'}$ being the screened Coulomb potential. In the case of the valley-independent out-of-plane spin polarization, the total effective magnetic fields

$$\mathbf{\Omega}^{\mu}_{\rm eff} = (\Omega_{\rm HF} + \mu\eta E_z)\mathbf{e}_{\hat{z}} \qquad (3)$$

have different values in the two valleys, leading to the valley-dependence of the out-of-plane spin relaxation.

In the present work, by utilizing the kinetic spin Bloch equation (KSBE) approach[48] with the hole-hole Coulomb, (both the intra- and intervalley) hole-phonon, and long-range hole-impurity scatterings included, we investigate the hole spin relaxation in BL WSe_2 due to the Rashba SOC [Eq. (1)]. In our investigation, the initial occupations of holes of each spin are identical in the two valleys. In the case of small spin polarization (i.e., weak HF effective magnetic field), the total effective magnetic fields [Eq. (3)] determined by the Zeeman-like fields, have identical absolute values in the two valleys. We investigate the temperature and hole density dependence of both the out-of- and in-plane spin relaxation times (SRTs), and show that for in-plane spins, the relaxation process is dominated by the intervalley spin relaxation channel induced by the Zeeman-like fields, and the contribution of the intervalley hole-phonon scattering becomes dominant. But for out-of-plane spin relaxation, the intervalley hole-phonon scattering is marginal, which indicates that out-of-plane spins relax independently in the two valleys. With the intervalley scattering removed, the out-of-plane SRTs τ^{μ}_{sz} in the strong scattering limit[49,51]

$$\tau^{\mu}_{sz} = \frac{1+(\Omega^{\mu}_{\rm eff}\tau_p)^2}{\langle\Omega^2_{\perp}(\mathbf{k})\rangle\tau_p} = \frac{1}{\langle\Omega^2_{\perp}(\mathbf{k})\rangle\tau_p} + \frac{|\Omega^{\mu}_{\rm eff}|^2}{\langle\Omega^2_{\perp}(\mathbf{k})\rangle}\tau_p, \qquad (4)$$

are identical in the two valleys due to the same absolute values of the total effective magnetic fields. Here, $\mathbf{\Omega}_{\perp}(\mathbf{k})$ and τ_p are the in-plane Rashba terms and momentum relaxation time due to the intravalley scattering, respectively.

In the case of large spin polarization (i.e., strong HF effective magnetic field), for in-plane spins, the SRT is insensitive to the spin polarization, similar to the case of ML MoS_2.[4] For out-of-plane spins, a large difference of the total effective magnetic fields [Eq. (3)] between the two valleys is obtained. We find that the intervalley hole-phonon scattering in this situation is weak at low temperature and low hole density, and hence the out-of-plane spins relax independently in the two valleys, leading to different SRTs [Eq. (4)]. The enhancement of the intervalley hole-phonon scattering by increasing temperature can suppress this difference in the SRTs. Moreover, the intervalley scattering also becomes stronger with the increase of hole density at low temperature, which originates from the different SRTs. Specifically, as shown in Fig. 1, when the HF effective magnetic field and Zeeman-like field have opposite directions, say, in the K valley, the smaller total effective magnetic field [Eq. (3)] leads to a faster SRT [Eq. (4)] in this valley. Over time, this faster spin relaxation makes the density for spin-down (-up) holes larger (smaller) than the corresponding one with the same spin in the K′ valley, triggering the intervalley scattering of spin-down (-up) holes from the K (K′) valley to the K′ (K) one by emitting phonons to suppress this density difference. With larger density difference by increasing the hole density, the intervalley scattering becomes stronger. In addition, due to the weak intravalley hole-phonon scattering at low temperature but relatively strong hole-hole Coulomb scattering, we find that the fast spin precessions result in a quasi hot-hole Fermi distribution characterized by an effective hot-hole temperature $T_{\rm eff}$ larger than the temperature T, which also enhances the intervalley scattering.

During above process, it is interesting to discover that the initially equal hole densities in the two valleys are broken in the temporal evolution, with more holes are accumulated in the K′ valley, leading to the build up of the valley polarization. This arises from the larger effective hot-hole temperature for spin-down holes than that for spin-up ones, which makes the spin-conserving intervalley scattering rate $\tau_{p\,\Downarrow}^{\rm K\to K'}$ of spin-down holes faster than that $\tau_{p\,\Uparrow}^{\rm K'\to K}$ of spin-up holes (see Fig. 1). Specifically, due to the large difference of Fermi energies of spin-up and -down holes, the Rashba SOC [Eq. (1)] near the Fermi energy of spin-up holes transfers holes from the spin-up states into the spin-down ones with the same energies, and hence more spin-down holes occupying the states with the energies higher than the corresponding

Fermi energy, leading to the larger effective hot-hole temperature. According to our calculation, with the experimental obtainable hole density and the spin polarization reaching 60 %, the accessible valley polarization can reach beyond 1 % which can last hundreds of picoseconds. In addition, due to the absence of electrons in the conduction bands in p-type BL WSe_2, the valley-depolarization induced by the exchange interaction[52] is absent here. Therefore, the valley polarization proposed above can be measured experimentally. This has not yet been reported in the literature.

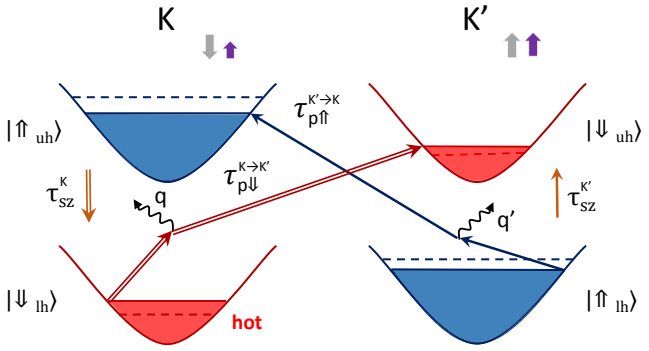

FIG. 1: (Color online) Schematic of the different spin relaxation processes in the two valleys and valley polarization process. In the figure, $|\Uparrow(\Downarrow)_{\rm uh(lh)}\rangle$ stands for the upper- (lower-) layer states for spin-up (-down) holes; the purple (gray) filled arrows, which have the same (opposite) directions in the two valleys, denote the HF (Zeeman-like) effective magnetic fields; the dashed lines stand for the initial occupations of holes of each spin. On one hand, this schematic shows that due to the smaller total effective magnetic field in the K valley, the SRT $\tau_{sz}^{\rm K}$ is faster than $\tau_{sz}^{\rm K'}$, which makes the density for spin-down (-up) holes in the K valley larger (smaller) than that in the K′ valley in the temporal evolution. On other hand, the intervalley scattering time $\tau_{p\Downarrow}^{\rm K\to K'}$ of spin-down holes is faster than that $\tau_{p\Uparrow}^{\rm K'\to K}$ of spin-up holes due to the larger effective hot-hole temperature for spin-down holes (red).

This paper is organized as follows. In Sec. II, we introduce our model and lay out the KSBEs. Then in Sec. III A, we investigate the temperature and the hole density dependence of the out-of-plane spin relaxation in BL WSe_2 with weak HF effective magnetic field. The anisotropy of the spin relaxation is also presented in this part. In Sec. III B, we show the influence of HF effective magnetic field when the large out-of-plane spin polarization is considered. The valley polarization due to the large spin polarization is also addressed in this part. We summarize in Sec. IV.

II. MODEL AND KSBES

In BL TMDs, in the presence of an external perpendicular electric field, the effective Hamiltonian of the lowest two hole bands near the K (K′) point can be written as[33]

$$H_{\rm eff}^{\mu}=\varepsilon_{\mu\mathbf{k}}+\mathbf{\Omega}^{\mu}\cdot\boldsymbol{\sigma}/2, \tag{5}$$

where $\varepsilon_{\mu\mathbf{k}}=\mathbf{k}^2/(2m^*)$, with m^* being the effective mass of the hole; the Rashba SOC $\mathbf{\Omega}^{\mu}$ is given in Eq. (1). However, the Rashba coefficients ν, α and η are absent in the literature. In this work, we use the ML Rashba SOC[53] in each layer to construct the BL Rashba SOC. Specifically, a hole in the lowest hole band in a given layer can first hop into the second layer by the spin-conserving interlayer hopping and then flip spin by the ML Rashba SOC to the lowest hole band in the second layer. Or the hole in the lowest hole band can first flip spin in the first layer and then hop to the second layer with same spin. The lowest two hole bands in BL TMDs, which have opposite spin polarizations, are then coupled with each other. Due to the large spin splitting of the hole bands in each layer, both the ML Rashba SOC and interlayer hopping can be treated perturbatively. We use the Löwdin partition method[54,55] to derive the effective Rashba SOC of the lowest two hole bands in BL TMDs, and obtain the Rashba coefficients, which are given in Appendix A in details.

The KSBEs are then written as[48,56,57]

$$\partial_t\rho_{\mu\mathbf{k}}=\partial_t\rho_{\mu\mathbf{k}}|_{\rm coh}+\partial_t\rho_{\mu\mathbf{k}}|_{\rm scat}, \tag{6}$$

where $\rho_{\mu\mathbf{k}}$ represent the density matrices of holes with the off-diagonal terms $\rho_{\mu\mathbf{k},\frac{1}{2}-\frac{1}{2}}=\rho^*_{\mu\mathbf{k},-\frac{1}{2}\frac{1}{2}}$ representing the spin coherence and the diagonal ones $\rho_{\mu\mathbf{k},\sigma\sigma}\equiv f_{\mu\mathbf{k},\sigma}$ ($\sigma=\pm\frac{1}{2}$) being the hole distribution functions. The coherent terms $\partial_t\rho_{\mu\mathbf{k}}|_{\rm coh}$ describe the spin precessions of holes due to the effective magnetic field $\mathbf{\Omega}^{\mu}$ and the HF effective magnetic field $\mathbf{\Omega}_{\rm HF}$. The scattering terms $\partial_t\rho_{\mu\mathbf{k}}|_{\rm scat}$ include the hole-hole Coulomb, long-range hole-impurity, intravalley hole-phonon and especially the intervalley hole-phonon scattering. The detailed expressions for the coherent and scattering terms can be found in Ref. 56. Particularly, the large Zeeman-like term $\mu\eta E_z$ in the Rashba SOC [Eq. (1)], leads to the energy-splitting of the lowest two hole bands in BL TMDs, which has opposite signs in the two valleys, and hence affects the spin-conserving intervalley hole-phonon scattering but has no effect on the intravalley scattering. By considering this energy-splitting, the intervalley scattering parts in the KSBEs are given by[48]

$$\partial_t\rho_{\mu\mathbf{k}}|^{\rm inter}_{\rm scat}=\left\{S_{\mu\mathbf{k}}(<,>)+S_{\mu\mathbf{k}}(<,>)^{\dagger}\right\}-\{<\leftrightarrow>\}, \tag{7}$$

with

$$S_{\mu\mathbf{k}}(>,<)=\pi\sum_{\mathbf{q}\mu'\eta_1\eta_2}|M^{\lambda}_{\mu\mu'\mathbf{q}}|^2\rho^{>}_{\mu'\mathbf{k}-\mathbf{q}}T_{\mu'\eta_1}T_{\mu\eta_2}\rho^{<}_{\mu\mathbf{k}}\big[N^{<}_{\mathbf{q}}\times\delta(\varepsilon_{\eta_2\mathbf{k}}-\varepsilon_{\eta_1\mathbf{k}-\mathbf{q}}+\omega_{\mathbf{q}})+N^{>}_{\mathbf{q}}\delta(\varepsilon_{\eta_1\mathbf{k}-\mathbf{q}}-\varepsilon_{\eta_2\mathbf{k}}+\omega_{\mathbf{q}})\big]. \tag{8}$$

Here, $N^{<}_{\mathbf{q}}=N_{\mathbf{q}}$ is the phonon distribution, $N^{>}_{\mathbf{q}}=N_{\mathbf{q}}+1$; $\rho^{<}_{\mu\mathbf{k}}=\rho_{\mu\mathbf{k}}$, and $\rho^{>}_{\mu\mathbf{k}}=1-\rho_{\mu\mathbf{k}}$; $\eta_1(\eta_2)=\pm1$ and $\varepsilon_{\pm1\mathbf{k}}=\varepsilon_{\mathbf{k}}\pm\eta E_z$; The projector operator reads $T_{\mu\eta}=$

$(1+\eta\mu\sigma_z)/2$; $|M^{\lambda}_{\mu\mu'\mathbf{q}}|^2$ is the scattering matrix element of the intervalley phonon mode λ.

However, the hole-phonon scattering matrix elements in BL TMDs have not yet been reported in the literature. For the intervalley hole-phonon scattering, with the intervalley scattering in each layer suppressed due to the large spin splitting,[1] holes in a given valley at a given layer are scattered into the other valley at different layer. We derive the matrix elements of this intervalley scattering by using the tight-binding model according to the arXiv version of the work by Viljas and Heikkilä.[58] We show that only the phonon modes $K_6^{\rm L}$ and $K_6^{\rm H}$ make the main contribution. Here, $K_6^{\rm L}$ ($K_6^{\rm H}$) is the phonon mode at the K point corresponding to the irreducible representation E_2'' of group C_{3h} with the lower (higher) phonon energy.[1] For the intravalley hole-phonon scattering, we derive the matrix elements of out-of-plane phonon according to the same work by Viljas and Heikkilä; the matrix elements of in-plane phonon in BL TMDs are constructed by using the ML ones, which have been reported in the work by Jin *et al.*.[59] The specific derivation of the hole-phonon scattering matrix elements is give in Appendix C.

The matrix elements of the hole-phonon scatterings including the intervalley $K_6^{\rm L}$ ($|M^{\rm K_6^L}_{\mu\mu'\mathbf{q}}|^2$) and $K_6^{\rm H}$ ($|M^{\rm K_6^H}_{\mu\mu'\mathbf{q}}|^2$) phonon scatterings and the intravalley in-plane acoustic (AC) ($|M^{\rm AC}_{\mu\mu'\mathbf{q}}|^2$), in-plane optical (OP) ($|M^{\rm E^2_{2g}}_{\mu\mu'\mathbf{q}}|^2$, $|M^{\rm E_{1u},E^1_{2g}}_{\mu\mu'\mathbf{q}}|^2$) and out-of-plane OP ($|M^{\rm B^2_{2g}}_{\mu\mu'\mathbf{q}}|^2$, $|M^{\rm A^2_{2u},B^1_{2g}}_{\mu\mu'\mathbf{q}}|^2$) phonon scatterings are given by

$$|M^{K_6^{\rm L}}_{\mu\mu'\mathbf{q}}|^2=\frac{t_\perp'}{2\rho\Omega_{{\rm K},K_6^{\rm L}}}\delta_{\mu',-\mu}, \tag{9}$$

$$|M^{K_6^{\rm H}}_{\mu\mu'\mathbf{q}}|^2=\frac{t_\perp'}{2\rho\Omega_{{\rm K},K_6^{\rm L}}}\frac{2M_{\rm M}}{M_{\rm X}}\delta_{\mu',-\mu}, \tag{10}$$

$$|M^{{\rm AC},E^2_{2g}}_{\mu\mu'\mathbf{q}}|^2=\frac{(\Xi)^2 q}{2\rho v_{\rm LA}}\delta_{\mu',\mu}, \tag{11}$$

$$|M^{B^2_{2g}}_{\mu\mu'\mathbf{q}}|^2=\frac{{t_\perp'}^2}{\rho\gamma q^2}\delta_{\mu',\mu}, \tag{12}$$

$$|M^{E_{1u},E^1_{2g}}_{\mu\mu'\mathbf{q}}|^2=\frac{(D_{\rm OP})^2}{\rho\Omega_{\Gamma,E_{1u}}}\delta_{\mu',\mu}, \tag{13}$$

$$|M^{A^2_{2u},B^1_{2g}}_{\mu\mu'\mathbf{q}}|^2=\frac{{t_\perp'}^2}{2\rho\Omega_{\Gamma,A^2_{2u}}}\frac{2M_d}{M_t}\delta_{\mu',\mu}, \tag{14}$$

where E^2_{2g}, B^2_{2g}, E_{1u}, E^1_{2g}, A^2_{2u}, B^1_{2g} are the phonon modes at the Γ point in BL TMDs;[60–63] $\Omega_{\Gamma({\rm K}),\lambda}$ is the energy of phonon mode λ at Γ(K) point; ρ is the mass density; $v_{\rm LA}$ is the sound velocity corresponding to longitudinal acoustic (LA) phonon; $\gamma=\sqrt{k_BT/(\rho v_0^2)}$ is the parameter for the energy dispersion of the out-of-plane AC phonon with v_0 being the corresponding sound velocity;[1] k_B represents the Boltzmann constant; $t_\perp'$ is the derivative of interlayer hopping $t_\perp$ with respect to the corresponding hopping bond length; Ξ and $D_{\rm OP}$ are the deformation potentials of the in-plane AC and OP phonon in ML TMDs,[59] respectively; $M_{\rm M}$ and $M_{\rm X}$ are the masses of the M atom and the X atom of the TMD MX_2, respectively. The remaining matrix elements of the hole-hole Coulomb and long-range hole-impurity scatterings can be found in the work by Wang and Wu.[4]

III. NUMERICAL RESULTS

TABLE I: Parameters for WSe_2 used in our calculation. Note that m_0 stands for the free electron mass.

ν (Å^2)	0.0342^a	η (Å)	1.06^a
m^*/m_0	0.51^b	α (Å)^2	-5.673^a
κ	5.20^c	$t_\perp'$ (eV/Å)	1.26^d
Ξ (eV)	2.1^e	$D_{\rm OP}$ (10^8 eV/cm)	3.1^e
$v_{\rm LA}$ (10^5 cm/s)	3.30^e	v_0 (10^5 cm/s)	2.24^c
$\Omega_{E_{1u}}$ (meV)	30.8^e	$\Omega_{A^2_{2u}}$ (meV)	38.51^f
$\Omega_{{\rm K},K_6^{\rm L}}$ (meV)	17.5^e	$\Omega_{{\rm K},K_6^H}$ (meV)	31.5^e
$M_{\rm Se}/M_{\rm W}$	0.429	ρ (10^{-7} g/cm^2)	6.6^c

[a] Appendix A. [b] Ref. 35. [c] Ref. 1. [d] Ref. 37. [e] Ref. 59. [f] Ref. 63.

In this work, we focused on the case of WSe_2. The initial occupations of holes of each spin are identical in the two valleys in our calculation. The spin-polarization direction is along the $\hat{z}$-axis unless otherwise specified. The long-range impurity density is taken to be $N_i=0.02N_h$ with N_h being the hole density. Then the corresponding mobility at $T=250$ K in our investigation is around 180 cm^2/(V·s), which agrees with those reported in the existing experiments.[64–66] All the material parameters used in our calculation are listed in Table I. With above parameters, by numerically solving the KSBEs, we discuss the spin relaxation at small and large spin polarizations (i.e., weak and strong HF effective magnetic fields) in Secs. III A and III B, respectively.

A. Weak HF effective magnetic field

In this subsection, the initial spin polarizations P_s in the two valleys are set to be 2.5 %, leading to the weak HF effective magnetic field ($|\Omega_{\rm HF}|\ll|\eta E_z|$) in our calculation. Then the out-of-plane SRTs τ^{μ}_{sz} due to the intravalley scatterings [given in Eq. (4) with $\Omega^{\mu}_{\rm eff}\approx\mu\eta E_z$], have identical values τ_{sz} in the two valleys. Moreover, owing to the competition between $[|\Omega^{\mu}_{\rm eff}|^2/\langle\Omega^2_\perp(\mathbf{k})\rangle]\tau_p$ and $[\langle\Omega^2_\perp(\mathbf{k})\rangle\tau_p]^{-1}$ in Eq. (4), the SRT can be divided into two regimes: regime I, the anomalous EY-like regime, where the first term makes a more important contribution and hence the SRT shows the EY-like behavior; regime II, the normal strong scattering regime, where the second term becomes more important. The crossover between regimes I and II is determined by $|\Omega_{\rm eff}\tau_p|=1$ with the system sitting in regime I (II) when $|\Omega_{\rm eff}\tau_p|>(<)1$. In this work, with $|\Omega_{\rm eff}|\approx|\eta E_z|$ at small spin polarization, we discuss the temperature and hole density dependence of the out-of-plane SRT at the small ($|\eta E_z\tau_p|\ll1$)

and medium ($|\eta E_z \tau_p| \approx 1$) fields. The large field with $|\eta E_z \tau_p| \gg 1$, which leads to a large energy-splitting of the hole bands similar to ML WSe_2, is not included in this work. We also investigate the anisotropic spin relaxation by varying the spin-polarization direction in this subsection.

1. *Temperature dependence of out-of-plane spin relaxation*

We first investigate the temperature dependence of the out-of-plane spin relaxation. The SRTs τ_{sz} as function of temperature T at different hole densities are plotted in Figs. 2 and 3 at the small ($E_z = 0.003$ V/Å) and medium ($E_z = 0.01$ V/Å) fields, respectively. All the relevant scatterings are included in the calculation. From Fig. 2, it is noted that the intervalley hole-phonon and the long-range hole-impurity scatterings are marginal to the out-of-plane spin relaxation, since the SRTs with both the intervalley and long-range hole-impurity scatterings (curve with open circles) removed are close to the one with all scatterings included (curve with squares). To further elucidate the role of the remaining hole-hole Coulomb and intravalley hole-phonon scatterings, we compare the SRT with only the hole-hole Coulomb scattering included (curve with crosses) and the one with only the intravalley hole-phonon scattering included (curve with dots). The hole-hole Coulomb scattering is found to be more important at low temperature since the SRT with only the hole-hole Coulomb scattering is much larger than the counterpart, while the intravalley hole-phonon scattering plays an important role at high temperature.

At the small field (the SRT is in regime II), a peak around $T = 60$ K at the hole density $N_h = 0.4\times10^{12}$ cm^{-2} (the Fermi temperature $T_F = 11$ K) is observed in the temperature dependence of the SRT [see Fig. 2(a)]. As revealed in the previous works,[56,67,68] this peak is due to the crossover of the hole-hole Coulomb scattering from the degenerate to nondegenerate limits [i.e., $1/\tau_p^{\rm hh} \propto \ln(T_F/T)T^2/T_F$ when $T \ll T_F$ and $1/\tau_p^{\rm hh} \propto 1/T$ when $T \gg T_F$][69,70] when the SRT is in the normal strong scattering regime. Unlike the previous studies in semiconductors, where the peak locations in different materials locate in the range $(T_F/4, 2T_F)$,[56,67,68,71–73] the peak location of p-type WSe_2 is around $5T_F$. Moreover, compared with the case with only the hole-hole Coulomb scattering, with all scatterings included, the peak is shifted toward a higher temperature at T_c^h for the low density and found to be destroyed (not shown) when $N_h \gtrsim 2\times10^{12}$ cm^{-2} ($5T_F \gtrsim 275$ K). This is due to the fact that the reduction of the Coulomb scattering in the nondegenerate limit can be compensated by the increase of the intravalley hole-phonon scattering, similar to the previous work,[56] and the intravally hole-phonon scattering is stronger than the hole-hole Coulomb scattering after 275 K. Consequently, when $N_h \gtrsim 2\times10^{12}$ cm^{-2}, the SRT increases with the decrease of τ_p by increasing temperature, as shown in Fig. 2(c) at $N_h = 2\times10^{13}$ cm^{-2}.

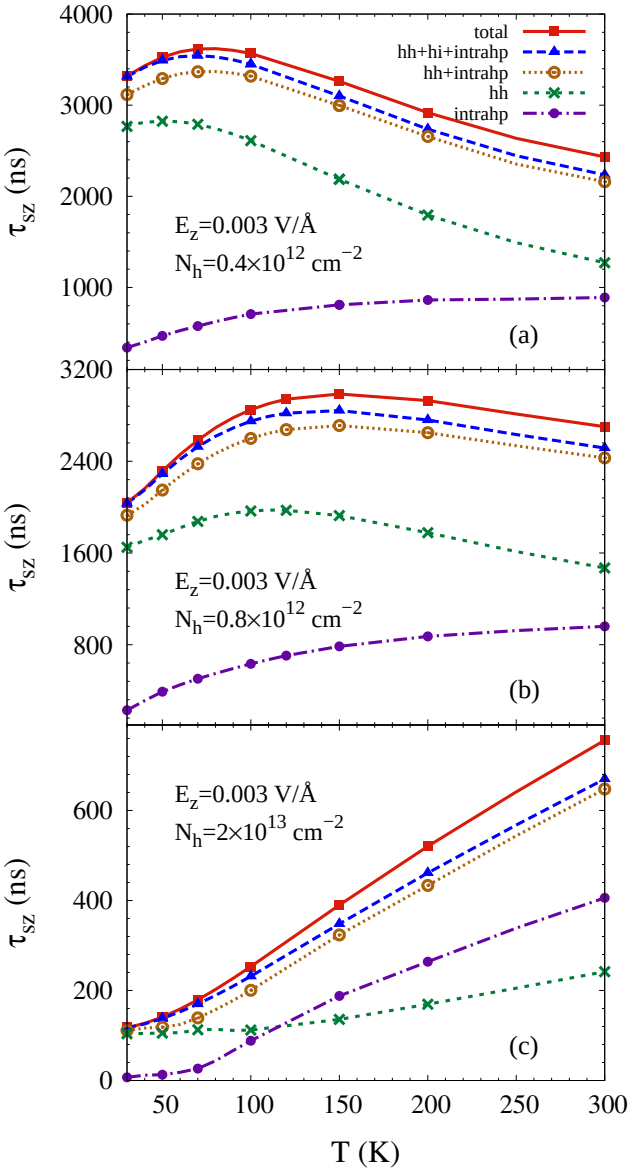

FIG. 2: (Color online) The SRTs τ_{sz} as function of T at (a) $N_h = 0.4\times10^{12}$ cm^{-2}, (b) $N_h = 0.8\times10^{12}$ cm^{-2}, and (c) $N_h = 2\times10^{13}$ cm^{-2}. Squares: all the relevant scatterings are included; Triangles: the intervalley hole-phonon scattering is removed; Open circles: both the intervalley hole-phonon and long-range hole-impurity scatterings are removed; Crosses (Dots): only the hole-hole Coulomb (intravalley hole-phonon) scattering is included. $E_z = 0.003$ V/Å.

At the medium field (see Fig. 3), the crossover between regimes I and II is observed at T_c^r. Specifically, with the increase of τ_p by removing each scattering at the same temperature, τ_{sz} increases in regime I while decreases in regime II. Compared with the location of T_c^h at the small field, which is determined by τ_p and

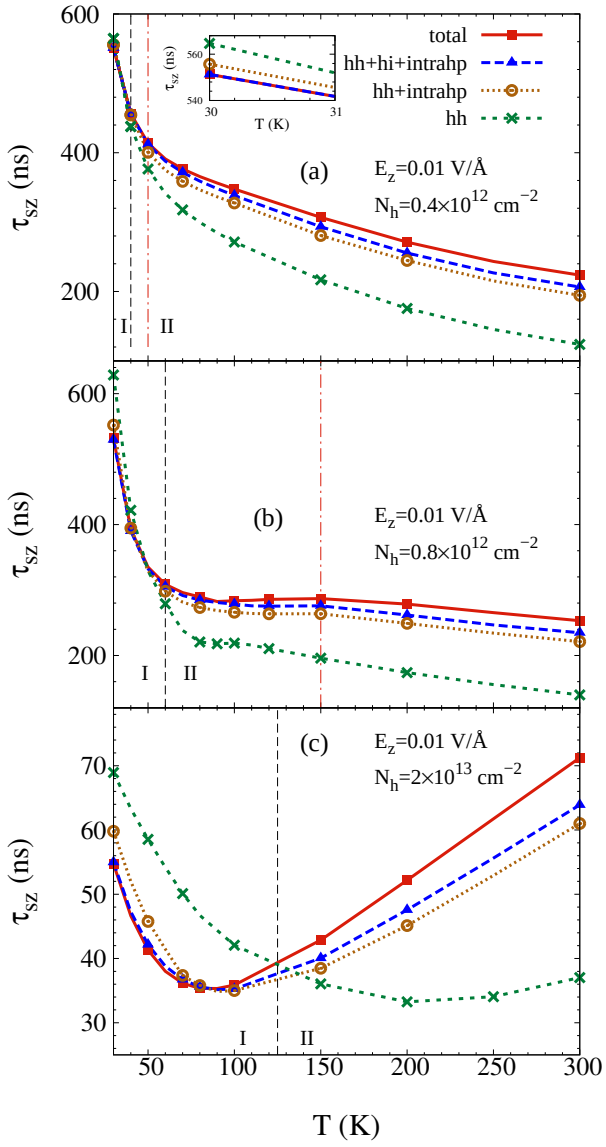

FIG. 3: (Color online) The SRTs τ_{sz} as function of T at (a) $N_h = 0.4\times10^{12}$ cm^{-2}, (b) $N_h = 0.8\times10^{12}$ cm^{-2}, and (c) $N_h = 2\times10^{13}$ cm^{-2}. Squares: all the relevant scatterings are included; Triangles: the intervalley hole-phonon scattering is removed; Open circles: both the intervalley hole-phonon and long-range hole-impurity scatterings are removed; Crosses: only the hole-hole Coulomb scattering is included. The inset in (a) zooms the temperature range 30-31 K. The vertical black dashed and red dash-dot lines indicate T_c^r and T_c^h, respectively. $E_z = 0.01$ V/Å.

not influenced by E_z, we find that the location of the crossover between regimes I and II T_c^r (indicated by the vertical black dashed line) is always smaller than T_c^h (indicated by the vertical red dash-dot line) at the corresponding hole density. This is because that with increasing temperature before T_c^h, the decrease of τ_p by the hole-hole Coulomb and intravalley hole-phonon scatterings leads to the crossover from regime I ($|\eta E_z \tau_p| > 1$) to II ($|\eta E_z \tau_p| < 1$). Therefore, with increasing temperature before T_c^h, the SRT in regime I ($\tau_{sz} \propto \tau_p$) decreases whereas in regime II ($\tau_{sz} \propto \tau_p^{-1}$) increases [see Fig. 3(b)]. Additionally, with increasing temperature after T_c^h (the SRT is entirely in regime II), as mentioned above, τ_p increases (decreases) when $N_h <$ (>)2×10^{12} cm^{-2}, and hence τ_{sz} decreases (increases), as shown in the figures. Consequently, when T_c^r is close to T_c^h, as shown in Fig. 3(a) at $N_h = 0.4\times10^{12}$ cm^{-2}, the peak existed at the previous small field with the same hole density is vanished here. But when T_c^r is separated from T_c^h, as shown in Fig. 3(b) at $N_h = 0.8\times10^{12}$ cm^{-2}, the peak existed at the small field with the identical hole density [Fig. 2(b)] is observed at the same temperature position here, but is less visible.

2. *Hole density dependence of out-of-plane spin relaxation*

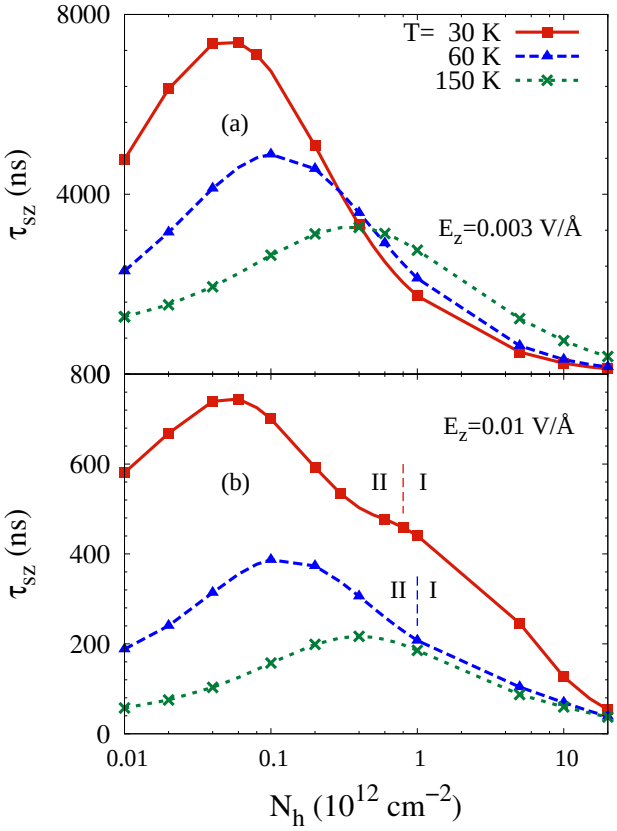

FIG. 4: (Color online) The SRTs τ_{sz} versus N_h at different temperatures with (a) $E_z = 0.003$ V/Å and (b) $E_z = 0.01$ V/Å. The vertical red (blue) dashed line indicates the crossover between regimes I and II at $T = 30$ (60) K.

Next we turn to study the hole density dependence

of out-of-plane spin relaxation. The SRTs τ_{sz} versus the hole density N_h at different temperatures are plotted in Figs. 4(a) and (b) at the small ($E_z = 0.003$ V/Å) and medium ($E_z = 0.01$ V/Å) fields, respectively. At the small field, a peak around $T_F{\approx}T/4.5$ is observed in the density dependence of the SRT, which is due to the crossover of holes from the nondegenerate to degenerate limits when the SRT is in the normal strong scattering regime.[68,71–73] At the medium field, similar peak is also observed, as shown in Fig. 4(b), indicating the SRT around $T_F{\approx}T/4.5$ still sits in regime II. But compared with the results at the small field, it is noted that the decrease of the SRT in the degenerate limit at the medium field slows down after $N_h = 0.8{\times}10^{12}\text{cm}^{-2}$ at $T = 30$ K (curve with squares). This arises from the crossover between regimes I and II. Specifically, with increasing the hole density in the degenerate limit at low temperature, the increase of $|\eta E_z \tau_p|$ due to the dominant hole-hole Coulomb scattering [i.e., $1/\tau_p^{\text{hh}} {\propto} \ln(T_F/T)T^2/T_F$ when $T_F {\gg} T$ ($T_F {\propto} N_h$ for the two-dimensional case)] drives the SRT from regime II ($|\eta E_z \tau_p| < 1$) to regime I ($|\eta E_z \tau_p| > 1$). In the degenerate limit, one has $\tau_{sz} {\propto} \ln(T_F/T)T^2/T_F^2$ in regime II whereas $\tau_{sz} {\propto} 1/[T^2 \ln(T_F/T)]$ in regime I since $\langle \Omega_\perp^2(\mathbf{k})\rangle {\propto} T_F$ in Eq. (4). Consequently, with the increase of N_h, the decrease of SRT slows down after the crossover. Similar behavior can also be observed at $T = 60$ K (curve with triangles). But at high temperature $T = 150$ K (curve with crosses), the intravalley hole-phonon scattering becomes stronger and the reduction of the Coulomb scattering in the degenerate limit can be compensated by the increase of the hole-phonon scattering, leading to the crossover indistinguishable.

3. *Anisotropic spin relaxation*

We also address the anisotropy of the spin relaxation with respect to the spin polarization direction. The temperature and hole density dependences of the in-plane spin relaxation along the $\hat{x}$-axis are plotted in Figs. 5 and 6, respectively. From Fig. 5, at the same hole density and temperature, the SRT with all the relevant scatterings included (solid curves with squares or triangles) is about four orders of magnitude smaller than the one with the intervalley hole-phonon scattering removed (dashed curves with dots or crosses), indicating the intervalley hole-phonon scattering makes a dominant contribution to the in-plane spin relaxation. This is very different from the previous results of the out-of-plane spin relaxation, where the intervalley hole-phonon scattering is marginal. Specifically, the Zeeman-like term, together with the intervalley hole-phonon scattering, opens an intervalley spin relaxation channel, as pointed out by Wang and Wu in ML MoS_2,[4,5] which dominates the in-plane spin relaxation in p-type BL WSe_2.

In addition, the SRTs decrease monotonically with the increase of temperature (see Fig. 5) or hole density (see Fig. 6) but are insensitive to the initial spin polarization

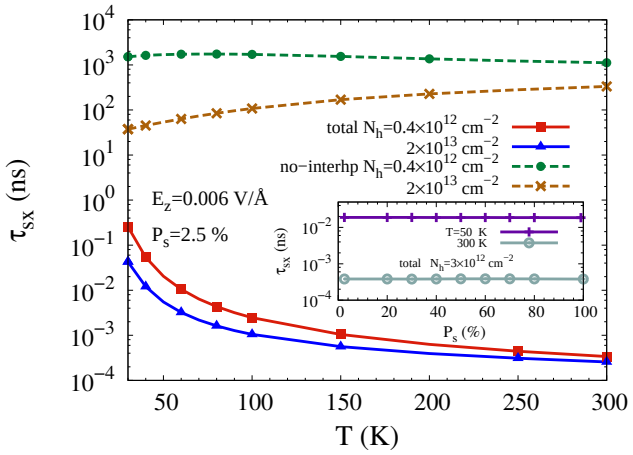

FIG. 5: (Color online) The SRTs τ_{sx} as function of T at different hole densities. $P_s = 2.5$ %. Solid curves: all the relevant scatterings are included; Dashed curves: the intervalley hole-phonon scattering is removed. The inset shows the SRTs versus initial spin polarization P_s at different temperatures when $N_h = 3{\times}10^{12}$ cm^{-2}. $E_z = 0.006$ V/Å.

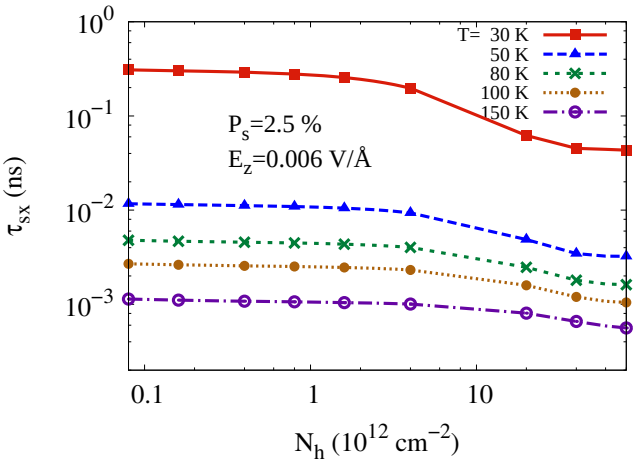

FIG. 6: (Color online) The SRT τ_{sx} versus hole density N_h at different temperatures. $P_s = 2.5$ %. $E_z = 0.006$ V/Å.

(see the inset in Fig. 5). This is due to the dominant intervalley spin relaxation channel, very similar to the case of ML MoS_2[4] when only the intervalley electron-phonon scattering is considered. Specifically, the intervalley hole-phonon scattering is in the weak-scattering limit, and hence the in-plane SRT $\tau_{sx} = \tau_p^{\text{inter}}$,[4,74] with τ_p^{inter} representing the intervalley hole-phonon scattering time. Consequently, the in-plane SRT decreases with the enhancement of the intervalley hole-phonon scattering as the temperature or hole density increases.

B. Strong HF effective magnetic field

1. *Spin polarization dependence of out-of-plane spin relaxation*

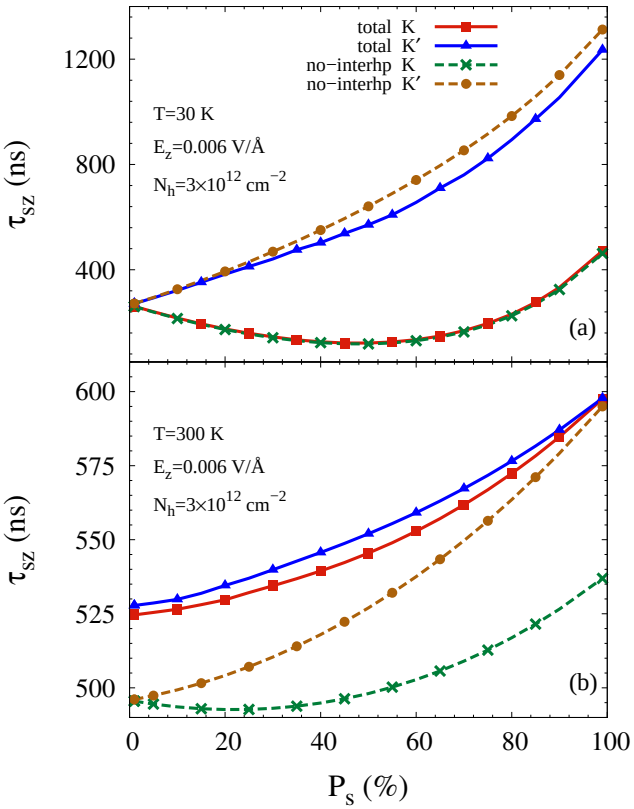

FIG. 7: (Color online) The SRTs τ_{sz} versus initial spin polarization P_s at (a) $T = 30$ K and (b) $T = 300$ K. Squares (Triangles): in the K (K′) valley with all the relevant scatterings included; Crosses (Dots): in the K (K′) valley with the intervalley hole-phonon scattering removed. $N_h = 3\times10^{12}$ cm^{-2}. $E_z = 0.006$ V/Å.

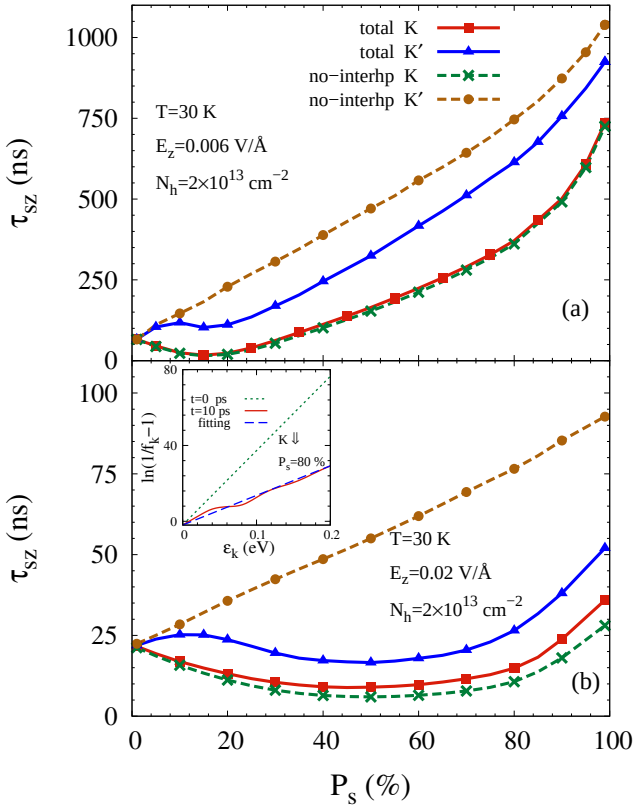

FIG. 8: (Color online) The SRTs τ_{sz} versus initial spin polarization P_s at (a) $E_z = 0.006$ V/Å and (b) $E_z = 0.02$ V/Å. Squares (Triangles): in the K (K′) valley with all the relevant scatterings included; Crosses (Dots): in the K (K′) valley with the intervalley hole-phonon scattering removed. The inset in (b) shows the distributions for spin-down holes in the K valley at $N_h = 2\times10^{13}$ cm^{-2} and initial spin polarization $P_s = 80$ % when $t = 0$ ps and $t = 10$ ps. $T = 30$ K. $N_h = 2\times10^{13}$ cm^{-2}.

At large spin polarization (i.e., strong HF effective magnetic field), different total effective magnetic fields [Eq. (3)] in the two valleys show up. The out-of-plane SRTs in the two valleys are plotted as function of the initial spin polarization P_s in Figs. 7 and 8 at different temperatures and hole densities. We first focus on the case with the intervalley hole-phonon scattering removed (dashed curves with crosses or dots), where the out-of-plane spins relax independently in the two valleys. As seen from the figures, different SRTs in the two valleys are obtained, which arise from the difference of the total effective magnetic fields in Eq. (4). Specifically, when the HF and Zeeman-like effective magnetic fields share the same direction, say, in the K′ valley, the total effective magnetic field $|\mathbf{\Omega}_{\rm eff}^{\rm K'}| = |\Omega_{\rm HF}| + |\eta E_z|$, and hence the SRT $\tau_{sz}^{\rm K'}$ (dashed curve with dots), proportional to $1+|\mathbf{\Omega}_{\rm eff}^{\rm K'}\tau_p|^2$ [see Eq. (4)], increases with increasing the spin polarization (i.e., HF effective magnetic field). Whereas in the K valley, which has opposite directions between the HF and Zeeman-like fields, the total effective magnetic field reads $|\mathbf{\Omega}_{\rm eff}^{\rm K}| = ||\eta E_z| - |\Omega_{\rm HF}||$, and hence the SRT $\tau_{sz}^{\rm K}$ (dashed curve with crosses), proportional to $1+|\mathbf{\Omega}_{\rm eff}^{\rm K}\tau_p|^2$, exhibits a minimum at $|\Omega_{\rm HF}| = |\eta E_z|$ in the spin polarization dependence. This minimum location in the spin polarization dependence can be tuned by the temperature [see the comparison between Figs. 7(a) and (b)], hole density [see the comparison between Fig. 7(a) and Fig. 8(a)] and electric field [see the comparison between Figs. 8(a) and (b)]. Additionally, due to the larger effective magnetic field in the K′ valley in the present configuration, $\tau_{sz}^{\rm K}$ is always faster than $\tau_{sz}^{\rm K'}$.

When the intervalley hole-phonon scattering is included (solid curves with squares or triangles), the above difference of the SRTs between the two valleys is suppressed. This is understood that the intervalley scattering suppresses the difference of the hole density of each spin between the two valleys. At low hole den-

sity and low temperature, the intervalley scattering is weak, leading to the marginal suppression on the difference between $\tau_{sz}^{\rm K}$ and $\tau_{sz}^{\rm K'}$, as shown in Fig 7(a) at $T = 30$ K and $N_h = 3{\times}10^{12}$ cm^{-2}. However, in contrast to this marginal suppression at $T = 30$ K, the suppression with the same hole density at high temperature is markedly strong, as shown in Fig. 7(b) at $T = 300$ K, where the SRTs with the intervalley hole-phonon scattering included are nearly identical in the two valleys. This arises from the enhanced intervalley hole-phonon scattering.

Moreover, even at low temperature $T = 30$ K, where the intervalley hole-phonon scattering by absorbing phonons is negligible, the suppression on the difference between $\tau_{sz}^{\rm K}$ and $\tau_{sz}^{\rm K'}$ becomes stronger with the increase of the hole density [see the comparison between Fig. 7(a) and Fig. 8(a)]. This arises from the different spin relaxation processes in the two valleys. Specifically, as shown in Fig. 1, in the temporal evolution, the faster spin relaxation in the K valley makes the Fermi energy for spin-down (-up) holes larger (smaller) than the corresponding one with the same spin in the K′ valley, and this difference of Fermi energies [given in Eq. (B13) in Appendix B] ,

$$\Delta E_F^{\Uparrow(\Downarrow)} = 0.25 P_s N_h / D_s (e^{-t/\tau_{sz}^{\rm K'}} - e^{-t/\tau_{sz}^{\rm K}}), \qquad (15)$$

with $\Delta E_F^{\Uparrow(\Downarrow)} = D_s(N_{\rm K'(K)}^{\Uparrow(\Downarrow)} - N_{\rm K(K')}^{\Uparrow(\Downarrow)})$ and D_s representing the density of states, triggers the intervalley scattering of spin-down holes from the K to the K′ valley by emitting phonons. In this situation, the intervalley scattering time of spin-down holes in the degenerate limit can be written as [given in Eq. (D4) in Appendix D]

$$\tau_{p\ \Downarrow(\Uparrow)}^{\rm K(K')\to K'(K)} = \tau_p^* (e^{\beta \Delta E^{\Downarrow(\Uparrow)}} - 1), \qquad (16)$$

for $\Delta E^{\Downarrow(\Uparrow)} > 0$. Here, $\Delta E^{\Downarrow(\Uparrow)} = \Omega_\xi - \Delta E_F^{\Uparrow(\Downarrow)}$ with Ω_ξ ($\xi = K_6^{\rm L}, K_6^{\rm H}$) standing for the intervalley phonon energy; $1/\tau_p^* = 2|M^\xi|^2 m^*$ with $|M^\xi|$ being the matrix element of the intervalley hole-phonon scattering. Focused on a specific case at $P_s = 60$ %, at low hole density $N_h = 3{\times}10^{12}$ cm^{-2} shown in Fig. 7(a), the difference of the Fermi energies between the two valleys ($\Delta E_F^{\Uparrow(\Downarrow)}|^{\rm max} \approx 3.3$ meV) is much smaller than the intervalley phonon energy ($\Omega_{{\rm K},K_6^{\rm L}} = 17.5$ meV), and hence the intervalley scattering by emitting phonons is blocked since $\beta \Delta E^{\Downarrow(\Uparrow)} \gg 1$. Nevertheless, with increasing the hole density to $N_h = 2{\times}10^{13}$ cm^{-2}, this difference over time ($\Delta E_F^{\Uparrow(\Downarrow)}|^{\rm max} \approx 15$ meV) becomes closer to the intervalley phonon energy, leading to the intervalley scattering by emitting phonons enhanced at nonzero temperature.

In addition, we find that the above suppression on the difference of the SRTs at low temperature can be further enhanced by increasing the electric field [see the comparison between Fig. 8(a) and (b)], which arises from a quasi hot-hole distribution. Specifically, as shown in the inset of Fig. 8(b), where the distributions for spin-down holes in the K valley at $t = 0$ ps (dash-dot curve) and $t = 10$ ps (solid curve) are plotted at the initial spin polarization $P_s = 80$ %. Due to the weak intravalley hole-phonon scattering at low temperature but relatively strong hole-hole Coulomb scattering, one finds that the fast spin precessions at a large electric field (i.e., a large Rashba SOC) result in a quasi hot-hole Fermi distribution characterized by an effective hot-hole temperature $T_{\rm eff}$ (the slope of the dashed curve is proportional to $T_{\rm eff}^{-1}$) larger than T (the slope of the dash-dot curve is proportional to T^{-1}), which enhances the intervalley hole-phonon scattering for spin-down holes by emitting phonons. Similar behaviors can also be observed for spin-up holes. With the enhanced intervalley hole-phonon scattering, the difference of the SRTs between the two valleys is further suppressed.

2. *Temperature dependence of out-of-plane spin relaxation*

The SRTs in the two valleys versus temperature T at different hole densities are plotted in Fig. 9 with a fixed large spin polarization $P_s = 55$ %. In the computation, the electric field is chosen at $|\eta E_z| = |\Omega_{\rm HF}|$ when $T = 30$ K, providing a large difference of the SRTs in the two valleys in the absence of the intervalley hole-phonon scattering.

At $N_h = 0.8{\times}10^{12}$ cm^{-2} shown in Fig. 9(a), for the case with the intervalley hole-phonon scattering removed, even at the small electric field ($E_z = 0.004$ V/Å), due to the large HF effective magnetic field ($|\Omega_{\rm HF}|/\eta = 0.0023$ V/Å at $T = 30$ K), the total effective magnetic field in the K′ valley ($|\Omega_{\rm eff}^{\rm K'}| = |\Omega_{\rm HF}| + |\eta E_z|$) is a medium field ($|\Omega_{\rm eff}^{\rm K'}\tau_p| \approx 1$) whereas that in the K valley ($|\Omega_{\rm eff}^{\rm K}| = ||\Omega_{\rm HF}| - |\eta E_z||$) is a small field ($|\Omega_{\rm eff}^{\rm K'}\tau_p| \ll 1$). Therefore, the behaviors of the SRTs originally existed at small spin polarization with the small (medium) total effective magnetic field [see Fig. 2(b) (3(b))] is observed in the K (K′) valley here [dashed curve with crosses (dots)]. In addition, the difference of the SRTs in the two valleys becomes weaker with the increase of temperature even when the intervalley hole-phonon scattering is removed. This is because the HF effective magnetic field becomes weaker with increasing temperature into the nondegenerate limit,[47] making the difference of the total effective magnetic fields between the two valleys much smaller. When the intervalley hole-phonon scattering is included (solid curves with squares or triangles), this difference of the SRTs is further suppressed and becomes nearly vanished when $T > 110$ K.

At the high hole density $N_h = 2{\times}10^{13}$ cm^{-2} as shown in Fig. 9(b), the HF effective magnetic field ($|\Omega_{\rm HF}|/\eta = 0.022$ V/Å at $T = 30$ K) is insensitive to the temperature in the degenerate limit, and hence the SRT in the K′ valley with the intervalley scattering removed is completely in regime I whereas that in the K valley sits in regime II. Consequently, with the decrease of τ_p by increasing temperature, the SRT increases in the K valley (dashed curve with crosses) but decreases in the K′ one (dashed curve

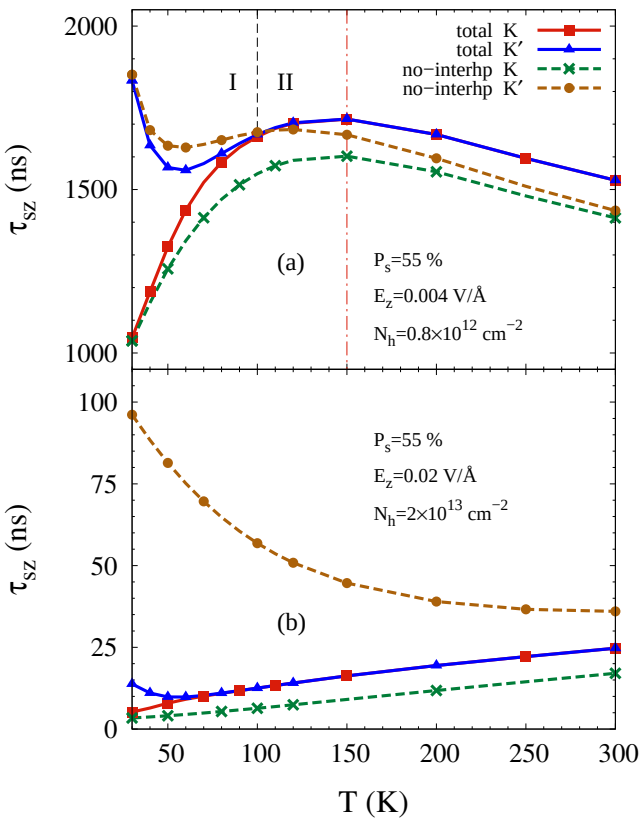

FIG. 9: (Color online) The SRT τ_{sz} versus temperature T at (a) $N_h = 0.8\times10^{12}$ cm^{-2} and $E_z = 0.004$ V/Å and (b) $N_h = 2\times10^{13}$ cm^{-2} and $E_z = 0.02$ V/Å. The initial spin polarization $P_s = 55$ %. Squares (Triangles): in the K (K′) valley with all the relevant scatterings included; Crosses (Dots): in the K (K′) valley with the intervalley hole-phonon scattering removed. The vertical black dashed and red dash-dot lines indicate T_c^r and T_c^h, respectively.

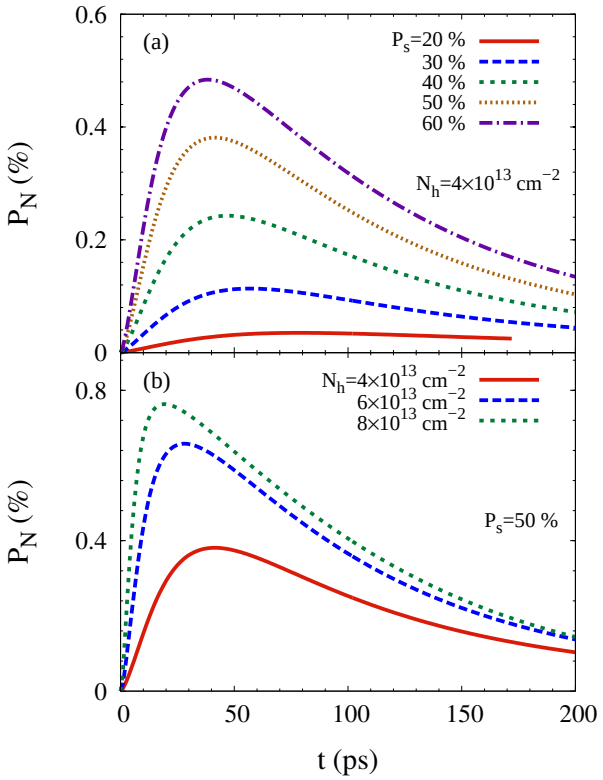

FIG. 10: (Color online) The temporal evolution of the valley polarization P_N with different hole densities N_h and initial spin polarizations P_s at $T = 50$ K.

with dots). When the intervalley hole-phonon scattering is included, even at low temperature, the difference of the SRTs is markedly suppressed, thanks to the enhanced intervalley scattering by emitting phonons as mentioned above.

3. *Valley polarization*

At large spin polarization and low temperature, it has been understood that the faster spin relaxation in the K valley makes the density for spin-down (-up) holes larger (smaller) than that with the same spin in the K′ valley, triggering the intervalley scattering of spin-down (-up) holes from the K (K′) to the K′ (K) valley by emitting phonons, as shown in Fig. 1. During this process, it is discovered that the initial equal occupations of holes in the two valleys are broken, leading to the build up of valley polarization. To realize the large difference of the spin relaxation processes with $\tau_s^{\rm K} \ll \tau_s^{\rm K'}$, the electric field in our calculation satisfies $\eta E_z = -\Omega_{\rm HF}|_{t=0}$ for given hole density and initial spin polarization, and then the temporal evolution of the valley polarization $P_N = (N_{\rm K'} - N_{\rm K})/N_h$ at different hole densities and initial spin polarizations when $T = 50$ K are plotted in Fig. 10. It is seen that over time, the valley polarization first increases and then decreases after reaching the maximum. This temporal dependence can be understood as follows.

By using the hot-hole Fermi distribution since the hole distribution in the temporal evolution exhibits as a quasi hot-hole Fermi distribution [see the inset in Fig. 8(b)], the temporal evolution of P_N in the degenerate limit can be written as [given in Eq. (D5) in Appendix D]

$$\frac{\partial P_N}{\partial t} = \frac{D_s}{N_h}\left(\frac{\Delta E^{\Downarrow}}{\tau_{p\,\Downarrow}^{\rm K\to K'}} - \frac{\Delta E^{\Uparrow}}{\tau_{p\,\Uparrow}^{\rm K'\to K}}\right). \tag{17}$$

Here, with $\Delta E^{\Downarrow(\Uparrow)} = \Omega_\xi - \Delta E_F^{\Downarrow(\Uparrow)}$, the intervalley scattering time $\tau_{p\,\Downarrow(\Uparrow)}^{\rm K(K')\to K'(K)}$ of spin-down (-up) holes is given in Eq. (16), but substituting T with the effective hot-hole temperature $T_{\rm eff}^{\Downarrow(\Uparrow)}$ of spin-down (-up) holes.

At the beginning of the temporal evolution, $\Delta E_F^{\Downarrow(\Uparrow)}|_{t=0} = 0$, and hence the intervalley scattering rate by emitting phonons $1/\tau_{p\,\Downarrow(\Uparrow)}^{\rm K(K')\to K'(K)} \approx 0$ [Eq. (16)] whereas the one by absorbing phonons is

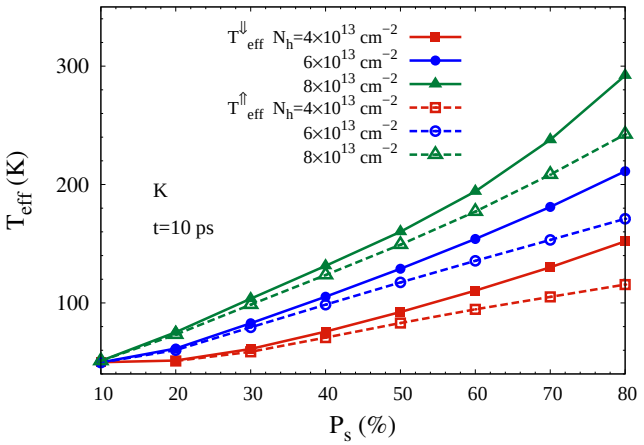

FIG. 11: (Color online) The effective hot-hole temperatures versus the initial spin polarization P_s at different hole densities when $t = 10$ ps. Solid (Dashed) curves: for spin-down (-up) holes in the K valley.

negligible at low temperature. Therefore, the out-of-plane spins relax independently in the two valleys with different SRTs $\tau_{sz}^{\rm K}$ and $\tau_{sz}^{\rm K'}$ [Eq. (4)]. Over time, due to the difference between $\tau_{sz}^{\rm K}$ and $\tau_{sz}^{\rm K'}$, $\Delta E_F^{\Downarrow(\Uparrow)}$ [Eq. (15)] increases with $\Delta E_F^{\Uparrow} = \Delta E_F^{\Downarrow}$, and then $1/\tau_{p\ \Downarrow(\Uparrow)}^{\rm K(K')\to K'(K)}$ becomes larger, meaning that the intervalley scattering by emitting phonons is triggered. Moreover, it is found that $\tau_{p\ \Downarrow}^{\rm K\to K'} < \tau_{p\ \Uparrow}^{\rm K'\to K}$, which arises from the larger effective hot-hole temperature for spin-down holes than that for spin-up ones. Specifically, the effective hot-hole temperatures for spin-down and -up holes in the K valley at different hole densities and initial spin polarizations when $t = 10$ ps are plotted in Fig. 11. $T_{\rm eff}^{\Uparrow(\Downarrow)}$ is found to increase with increasing the hole density or spin polarization due to the larger Fermi energy difference between spin-up and -down holes and the enhanced electric field ($|\eta E_z| = |\Omega_{\rm HF}|_{t=0}$). Furthermore, it is seen that $T_{\rm eff}^{\Downarrow}$ is always larger than $T_{\rm eff}^{\Uparrow}$, which arises from that the spin precession at large spin polarization brings more spin-down holes occupying the states with the energies higher than the corresponding Fermi energy. Similar behaviors can also be observed in the K′ valley. Consequently, with $\tau_{p\ \Downarrow}^{\rm K\to K'} < \tau_{p\ \Uparrow}^{\rm K'\to K}$ and $\Delta E_F^{\Uparrow} = \Delta E_F^{\Downarrow}$, one has $\partial_t P_N > 0$ in Eq. (17), leading to the increase of the valley polarization at the first tens of picosecond.

With further increase of time, the spin polarization (i.e., the HF effective magnetic field) becomes smaller due to the spin relaxation, leading to the decrease of the difference between $\tau_{sz}^{\rm K}$ and $\tau_{sz}^{\rm K'}$ by reducing the difference between $|\Omega_{\rm eff}^{\rm K}|$ and $|\Omega_{\rm eff}^{\rm K'}|$. Then $\Delta E_F^{\Uparrow(\Downarrow)}$ induced by different $\tau_{sz}^{\rm K}$ and $\tau_{sz}^{\rm K'}$ at the first tens of picosecond is suppressed by the intervalley scattering, and hence P_N decreases since $P_N N_h = D_s(\Delta E_F^{\Uparrow} - \Delta E_F^{\Downarrow})$. Moreover, with $P_N > 0$, $\Delta E_F^{\Uparrow}$ is relatively larger than $\Delta E_F^{\Downarrow}$, and hence one has $\tau_{p\ \Uparrow}^{\rm K'\to K} < \tau_{p\ \Downarrow}^{\rm K\to K'}$ from Eq. (16) since the difference between $T_{\rm eff}^{\Uparrow}$ and $T_{\rm eff}^{\Downarrow}$ (see Fig. 11) becomes smaller at the smaller spin polarization over time. Consequently, with the fact that the difference between $\tau_{p\ \Downarrow}^{\rm K\to K'}$ and $\tau_{p\ \Uparrow}^{\rm K'\to K}$ makes the dominant contribution in Eq. (17), one has $\partial_t P_N < 0$, leading to the decrease of the valley polarization after reaching the maximum.

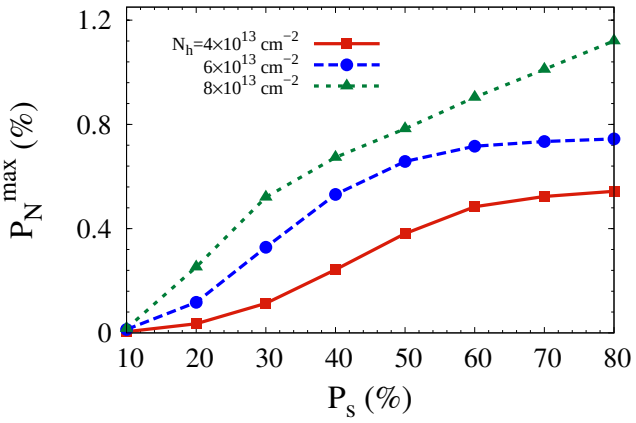

FIG. 12: (Color online) The maxima of the valley polarization P_N^m versus the initial spin polarization P_s at different hole densities.

The maxima of the valley polarization P_N^m are plotted in Fig. 12 at different hole densities and initial spin polarizations. It is discovered that this maximum increases with increasing the hole density and/or initial spin polarization. This dependence can be understood from the following analysis. As demonstrated above, the intervalley hole-phonon scattering suppresses the difference of the SRTs in the two valleys [see Fig. 7(c)]. By taking into account this suppression, from the KSBEs, the maximum P_N^m of the valley polarization is written as [given in Appendix D]

$$P_N^m = \left[\frac{F}{2}\frac{\tau_p^*}{N_h}\left(\frac{N_{\rm K}^{\Uparrow} - N_{\rm K}^{\Downarrow}}{\tau_{sz}^{\rm K}} - \frac{N_{\rm K'}^{\Uparrow} - N_{\rm K'}^{\Downarrow}}{\tau_{sz}^{\rm K'}}\right)\right]\Big|_{t=t_m}. \quad (18)$$

Here, the prefactor $F = (e^{\beta_{\rm eff}^{\Uparrow}\Omega_\xi}/\beta_{\rm eff}^{\Uparrow} - e^{\beta_{\rm eff}^{\Downarrow}\Omega_\xi}/\beta_{\rm eff}^{\Downarrow})/\Omega_\xi$; t_m is the time when the valley polarization reaches the maximum. To elucidate the trend of P_N^m with increasing initial spin polarization and hole density, we consider $t_m \approx 0$ approximately since t_m (around tens of picosecond) is much smaller than the SRT (larger than hundreds of picosecond). Then with $\Omega_{\rm eff}^{\rm K'}|_{t=0} = 2\eta E_z$ and $\Omega_{\rm eff}^{\rm K}|_{t=0} = 0$ in Eq. (4), an estimation of P_N^m can be written as

$$P_N^m \approx F|_{t=t_m}\frac{P_s}{4}\frac{\tau_p^*}{\tau_{sz}^{\rm K}}\left(1 - \frac{1}{1+4|\eta E_z \tau_p|^2}\right). \quad (19)$$

Therefore, with the increase of hole density or initial spin polarization and hence the electric field ($\eta E_z = -\Omega_{\rm HF}|_{t=0}$), $\tau_{sz}^{\rm K}$ becomes faster, and P_N^m tends to increase.

IV. SUMMARY

In summary, we have investigated the hole spin relaxation due to the Rashba SOC induced by an external perpendicular electric field in BL WSe_2, with all the relevant scatterings included. The Rashba SOC in BL WSe_2 is constructed from the ML Rashba SOC in each layer. Different from ML Rashba SOC, the out-of-plane component of the BL Rashba SOC acts as opposite Zeeman-like fields in the two valleys. For in-plane spins, this Zeeman-like field, opens an intervalley spin relaxation channel in the presence of the intervalley hole-phonon scattering, similar to the case of ML MoS_2[4,5] due to the intrinsic SOC. For out-of-plane spins, this Zeeman-like field is superimposed by the identical HF effective magnetic fields in the two valleys, and hence the valley with same (opposite) directions between these two fields has a larger (smaller) total effective magnetic field. Situations of weak and strong HF effective magnetic fields (i.e., small and large spin polarizations) are both considered. This difference of the total effective magnetic fields between two valleys greatly enriches the physics of the spin and valley dynamics in BL WSe_2.

In the case of small out-of-plane spin polarization, the total effective magnetic field $\Omega^{\mu}_{\rm eff}$ is determined by the Zeeman-like field $\mu\eta E_z$. We find that the intervalley hole-phonon scattering is marginal to the spin relaxation, indicating that the out-of-plane spins relax independently in the two valleys. Identical SRTs in the two valleys are obtained. We find that the behavior of the SRT is very sensitive to the electric field, and the different τ_p dependences of the SRT are observed at different electric fields. Specifically, the SRT can be divided into two regimes: regime I, the anomalous EY-like regime ($\tau_{sz} \propto \tau_p$) when $|\Omega_{\rm eff}\tau_p| > 1$; regime II, the normal strong scattering regime ($\tau_{sz} \propto \tau_p^{-1}$) when $|\Omega_{\rm eff}\tau_p| < 1$. In regime II, the peak in the temperature (density) dependence due to the crossover from the degenerate to the nondegenerate limit is observed, similar to the studies in semiconductors.[56,67,68,71–73] By increasing the electric field (i.e., total effective magnetic field) to a medium one ($|\Omega_{\rm eff}\tau_p|\approx 1$), the crossover between regimes I and II is observed. At this medium field, the peak in the temperature dependence vanishes when the crossover between regimes I and II is close to the crossover from the degenerate to the nondegenerate limit, whereas the peak in the hole density dependence is always observed. This arises from the different τ_p dependences of the SRT between regimes I and II.

In the case of large out-of-plane spin polarization (i.e., strong HF effective magnetic field), a large difference of the total effective magnetic fields between two valleys is obtained. Due to this difference, different out-of-plane SRTs in the two valleys are observed when the intervalley hole-phonon scattering is weak at low temperature and low hole density. Specifically, the SRT in the valley with the smaller total effective magnetic field is faster than that in the other valley. Moreover, by tuning the Zeeman-like and HF effective magnetic fields, the valley with the larger total effective magnetic field can fall into regime I ($|\Omega_{\rm eff}\tau_p| > 1$) while the other valley in regime II ($|\Omega_{\rm eff}\tau_p| < 1$), and hence the different behaviors of the SRTs between regimes I and II can be observed in the different valleys simultaneously. This difference of the SRTs between two valleys can be markedly suppressed through enhancing the intervalley hole-phonon scattering by increasing temperature or hole density. Additionally, at low temperature in the degenerate limit, due to the weak intravalley hole-phonon scattering but relatively strong hole-hole Coulomb scattering, the fast spin precessions result in a quasi hot-hole Fermi distribution characterized by an effective hot-hole temperature $T_{\rm eff}$ larger than T, which also enhances the intervalley hole-phonon scattering to suppress the difference of the SRTs.

It is interesting to discover that at large spin polarization and low temperature in the degenerate limit, the initially equal hole densities in the two valleys are broken in the temporal evolution, and a valley polarization is built up. This arises from the different spin relaxation processes in the two valleys at large spin polarizations. Specifically, in the temporal evolution, the different spin relaxation processes lead to different hole densities of each spin between the K and the K′ valleys, but with opposite signs between spin-up and -down holes. Therefore, the spin-conserving intervalley hole-phonon scattering, which transfers holes from the high density valley into the low density one, has opposite scattering directions between spin-down and -up holes. In addition, the effective hot-hole temperatures for spin-up and -down holes are found to be different, leading to different spin-conserving intervalley scattering rates. Consequently, with the different intervalley scattering rates in the two opposite scattering directions, the initial equal occupations of holes in the two valleys are broken, inducing the valley polarization.

Different from the out-of-plane spin relaxation where the intervalley hole-phonon scattering is marginal at small spin polarization but makes an important contribution at large one, for in-plane spin relaxation, the SRT is found to be insensitive to the spin polarization and the intervalley hole-phonon scattering always makes the dominant contribution even at low temperature. This arises from the intervalley spin relaxation channel induced by the Zeeman-like field in the presence of the intervalley hole-phonon scattering, similar to the case of ML MoS_2,[4] and this intervalley channel dominates the in-plane hole spin relaxation in BL WSe_2.

Acknowledgments

This work was supported by the National Natural Science Foundation of China under Grant No. 11334014, the National Basic Research Program of China under Grant No. 2012CB922002, and the Strategic Priority Research Program of the Chinese Academy of Sciences

under Grant No. XDB01000000. One of the authors (M.W.W) would like to thank Takashi Kimura at Kyushu University for hospitality where the work is finished. We acknowledge Y. Song and H. Dery for providing the identification of the K_6 phonon modes in the phonon energy spectrum.

Appendix A: Rashba SOC in BL TMDs

Due to the weak interlayer coupling in BL TMDs, we use the ML Rashba SOC[53] in each layer to construct the BL Rashba SOC. The ML Rashba SOC by Kormányos *et al.*[53] can be written as

$$H_{\rm Rashba}^{\rm ML}=\gamma_R(k_x\sigma_y-k_y\sigma_x)E_z, \tag{A1}$$

where σ_j ($j=x,y$) are the Pauli matrices for the real spin; the ML Rashba coefficients γ_R can be extracted from the electric field dependence of the effective mass in the work by Zibouche *et al.*,[75] which are given in Table II.

TABLE II: Rashba parameters of electrons γ_R^e and holes γ_R^h for ML MoS_2, WS_2, $MoSe_2$ and WSe_2, with the unit being Å^2.

	MoS_2	WS_2	$MoSe_2$	WSe_2
γ_R^e	0.0030	0.0326	0.0110	0.0416
γ_R^h	0.0410	0.1072	0.0422	0.1166

In BL TMDs, the Hamiltonian of the lowest four hole bands in the two layers near the K (K′) point by Gong *et al.*[35] reads

$$H_v^{\rm BL}=\varepsilon_{\mu\mathbf{k}}+\lambda_v(1+\mu\tau_z\sigma_z)/2+t_{\perp k}\tau_x. \tag{A2}$$

Here, λ_v is the spin splitting of the lowest two hole bands in each layer; $t_{\perp k}=t_\perp(1-a^2t^2k^2/\Delta^2)$ with $t_\perp$ and t representing the interlayer and nearest-neighbor intralayer hopping, respectively; τ_i stands for the Pauli matrices for layer pseudospin; a and Δ are the lattice constant and band gap, respectively. The specific values of these parameters are taken from Ref. 35.

In the presence of an external perpendicular electric field, the total hole Hamiltonian near the K (K′) point in BL TMDs reads

$$\begin{aligned}H_v &= \varepsilon_{\mu\mathbf{k}}+\lambda_v(1+\mu\tau_z\sigma_z)/2+t_{\perp k}\tau_x\\ &\quad+\big[\eta\tau_z+\gamma_R(k_x\sigma_y-k_y\sigma_x)\big]E_z,\end{aligned} \tag{A3}$$

where the electric dipole coefficient η can be obtained from the energy splitting of the lowest hole bands in the work by Zibouche *et al.*.[76]

By treating the ML Rashba SOC and the interlayer hopping as perturbations due to the large energy splitting λ_v in each layer, we construct the effective Hamiltonian by keeping the lowest two hole bands in two layers through the Löwdin partition method.[54,55] Up to the third order of the momentum, the effective hole Hamiltonian, which is consistent with the work by Yuan *et al.*[33] is written as

$$H_v=\varepsilon_{\mu\mathbf{k}}+E_z[\nu_k(k_x\sigma_y-k_y\sigma_x)+\mu\eta\sigma_z], \tag{A4}$$

where $\nu_k=\nu(1+\alpha k^2)$ with $\nu=\gamma_{\rm R}t_\perp/\lambda_v$ and $\alpha=-a^2t^2/\Delta^2$.

Appendix B: Derivation of Eq. (4)

We derive Eq. (4) based on the KSBEs in the presence of the out-of-plane total effective magnetic field (along the $\hat{z}$-axis) with only the long-range hole-impurity scattering included. In the derivation, we transform the KSBEs into the interaction picture, and further use the strong-scattering approximation.

The KSBEs in the collinear space with only the long-range hole-impurity scattering included can be written as

$$\begin{aligned}\partial_t\rho_{\mu\mathbf{k}} &= i\nu_k\big[k_y\sigma_x/2-k_x\sigma_y/2,\rho_{\mu\mathbf{k}}\big]-i\Omega_{\rm eff}^{\mu}\big[\sigma_z/2,\rho_{\mu\mathbf{k}}\big]\\ &\quad-2\pi N_i\sum_{\mathbf{k}'}|V_{\mathbf{k}-\mathbf{k}'}|^2\delta(\varepsilon_{\mathbf{k}}-\varepsilon_{\mathbf{k}'})(\rho_{\mu\mathbf{k}}-\rho_{\mu\mathbf{k}'}).\end{aligned} \tag{B1}$$

By transforming the density matrix into the interaction picture as

$$\widetilde{\rho}_{\mu\mathbf{k}} = \exp(i\Omega_{\rm eff}^{\mu}\sigma_z/2)\rho_{\mu\mathbf{k}}\exp(-i\Omega_{\rm eff}^{\mu}\sigma_z/2), \tag{B2}$$

the KSBEs in the interaction picture become

$$\begin{aligned}\partial_t\widetilde{\rho}_{\mu\mathbf{k}} &= i\nu_k\big[k_y\widetilde{\sigma}_x/2-k_x\widetilde{\sigma}_y/2,\widetilde{\rho}_{\mu\mathbf{k}}\big]-2\pi N_i\\ &\quad\times\sum_{\mathbf{k}'}|V_{\mathbf{k}-\mathbf{k}'}|^2\delta(\varepsilon_{\mathbf{k}}-\varepsilon_{\mathbf{k}'})(\widetilde{\rho}_{\mu\mathbf{k}}-\widetilde{\rho}_{\mu\mathbf{k}'}),\end{aligned} \tag{B3}$$

with $\widetilde{\sigma}_i=\exp(i\Omega_{\rm eff}^{\mu}\sigma_z/2)\sigma_i\exp(-i\Omega_{\rm eff}^{\mu}\sigma_z/2)$. After the Fourier transformation

$$\widetilde{\rho}_{\mu\mathbf{k}}^{l}=\frac{1}{2\pi}\int_0^{2\pi}d\theta_{\mathbf{k}}\widetilde{\rho}_{\mu\mathbf{k}}\exp(-il\theta_{\mathbf{k}}), \tag{B4}$$

one gets

$$\partial_t\widetilde{\rho}_{\mu\mathbf{k}}^{l}=-\nu_k k/4\big(\big[\widetilde{\sigma}_+,\widetilde{\rho}_{\mu\mathbf{k}}^{l-1}\big]-\big[\widetilde{\sigma}_-,\widetilde{\rho}_{\mu\mathbf{k}}^{l+1}\big]\big)-\widetilde{\rho}_{\mu\mathbf{k}}^{l}/\tau_{k,l}, \tag{B5}$$

with

$$\frac{1}{\tau_{k,l}}=\frac{m^*N_i}{2\pi}\int_0^{2\pi}d\theta_{\mathbf{q}}|V_{\mathbf{q}}|^2(1-\cos l\theta). \tag{B6}$$

Further keeping terms $|l|\leq1$ and defining the spin vector,

$$\widetilde{\mathbf{S}}_{\mu\mathbf{k}}^{l}=\mathrm{Tr}\big[\widetilde{\rho}_{\mu\mathbf{k}}^{l}\boldsymbol{\sigma}\big], \tag{B7}$$

one obtains

$$\begin{aligned}&\big[\tau_{k,1}^2\partial_t^3+2\tau_k^1\partial_t^2+(1+|\Omega_{\rm eff}^{\mu}\tau_{k,1}|^2)\partial_t+\nu_k^2k^2\tau_{k,1}^2\partial_t\\ &+\nu_k^2k^2\tau_{k,1}\big]\widetilde{S}_{\mu\mathbf{k}z}^{0}(t)=i\Omega_{\rm eff}^{\mu}(\nu_k^2k^2\tau_{k,1}^2).\end{aligned} \tag{B8}$$

In the strong scattering limit ($|\nu_k k\tau_{k,1}|^2 \ll 1$), Eq. (B8) becomes

$$\left[2\tau_{k,1}\partial_t^2 + (1+|\Omega^{\mu}_{\rm eff}\tau_{k,1}|^2)\partial_t + \nu_k^2 k^2 \tau_{k,1}\right]\widetilde{S}^0_{\mu\mathbf{k}z}(t) = 0. \quad \text{(B9)}$$

With the initial condition $\partial_t \widetilde{S}^0_{\mu\mathbf{k}z}(0) = 0$, the solution of $\widetilde{S}^0_{\mu\mathbf{k}z}(t)$ is given by

$$\widetilde{S}^0_{\mathbf{k}z}(t) = \frac{\widetilde{S}^0_{\mathbf{k}z}(0)}{2}\left\{(1+\frac{1}{\sqrt{1-c_z^2}})\exp\left[-\frac{t(1-\sqrt{1-c_z^2})}{4\tau_{k,1}/(1+|\Omega^{\mu}_{\rm eff}\tau_{k,1}|^2)}\right] + (1-\frac{1}{\sqrt{1-c_z^2}})\exp\left[-\frac{t(1+\sqrt{1-c_z^2})}{4\tau_{k,1}/(1+|\Omega^{\mu}_{\rm eff}\tau_{k,1}|^2)}\right]\right\}, \quad \text{(B10)}$$

with $c_z = 2\sqrt{2}\nu_k k\tau_{k,1}/(1+|\Omega^{\mu}_{\rm eff}\tau_{k,1}|^2)$. In the strong scattering limit ($c_z \ll 1$), one has

$$\widetilde{S}^0_{\mu\mathbf{k}z}(t) = \widetilde{S}^0_{\mu\mathbf{k}z}(0)\exp\big(-\frac{t}{8\tau_{k,1}/c_z^2}\big). \quad \text{(B11)}$$

The out-of-plane SRT is therefore

$$\tau^{\mu}_{sz} \approx (1+|\Omega^{\mu}_{\rm eff}\tau_{k,1}|^2)/(\nu_k^2 k^2 \tau_{k,1}). \quad \text{(B12)}$$

When all the relevant intravalley scatterings are included, by replacing $\tau_{k,1}$ with τ_p, Eq. (B12) becomes Eq. (4).

Moreover, without the intervalley scattering included, from Eq. (B11), the density difference of holes of each spin [$N_\mu = {\rm Tr}(\rho_{\mu\mathbf{k}})$] between the two valleys induced by the different SRTs can be written into

$$\Delta N_h^{\Uparrow(\Downarrow)} = 0.25 P_s N_h (e^{-t/\tau^{\rm K'}_{sz}} - e^{-t/\tau^{\rm K}_{sz}}). \quad \text{(B13)}$$

Appendix C: The hole-phonon scattering matrix elements

For the intravalley hole-phonon scattering, a symmetry group analysis of lattice vibrations at the Γ point, which belongs to the space group D_{6h}, has been performed in the previous work.[60] The decomposition into irreducible representations is as follows:

$$\begin{aligned}\Gamma \;=\; & A_{1g}\oplus 2A_{2u}\oplus B_{1u}\oplus 2B_{2g} \\ & \oplus E_{1g}\oplus 2E_{1u}\oplus E_{2u}\oplus 2E_{2g}. \end{aligned} \quad \text{(C1)}$$

The vibration pattern of these phonon modes can be found in Refs. 60–63. It is noted that only the modes [including in-plane OP ($E_{1u}, E^{1,2}_{2g}$) and AC (E^2_{1u}) phonons and out-of-plane OP (A^2_{2u}, $B^{1,2}_{2g}$) and AC (A^1_{2u}) phonons], which induce the vibrations of the transition metal atoms, can trigger the hole-phonon scattering.

Due to the weak interlayer coupling in BL TMDs,[60] the BL phonon vibrations are thought to consist of the corresponding ML phonon vibrations in each layer, and the BL phonon energy spectrum is close to the corresponding ML one.[40] Therefore, for the in-plane phonons, the BL intravalley hole-phonon scattering matrix elements are constructed by using the ML ones, which have been reported in the work by Jin *et al.*.[59] By considering the number of the in-plane phonon modes in BL TMDs, the scattering matrix elements are given by

$$|M^{{\rm AC},E^1_{2g}}_{\mu\mu'\mathbf{q}}|^2 = \frac{(\Xi)^2 q}{2\rho v_{\rm LA}}\delta_{\mu',\mu}, \quad \text{(C2)}$$

$$|M^{E_{1u},E^1_{2g}}_{\mu\mu'\mathbf{q}}|^2 = \frac{(D_{\rm OP})^2}{\rho\Omega_{\Gamma,E_{1u}}}\delta_{\mu',\mu}. \quad \text{(C3)}$$

But for the out-of-plane phonons, it has been shown that the contribution of the out-of-plane phonons in the hole-phonon scattering is marginal in ML TMDs.[59] However, the out-of-plane OP phonons (A^2_{2u}, B^1_{2g}) in BL TMDs, which induce the relative out-of-plane vibrations of the transition metal atoms in the two layers, can largely influence the variety of the interlayer hopping, triggering the intravalley hole-phonon scattering. By using the tight-binding model according to the arXiv version of the work by Viljas and Heikkilä,[58] we derived the matrix elements of this kind of hole-phonon scattering

$$|M^{B^2_{2g}}_{\mu\mu'\mathbf{q}}|^2 = \frac{{t'_\perp}^2}{\rho\gamma q^2}\delta_{\mu',\mu}, \quad \text{(C4)}$$

$$|M^{A^2_{2u},B^1_{2g}}_{\mu\mu'\mathbf{q}}|^2 = \frac{{t'_\perp}^2}{2\rho\Omega_{\Gamma,A^2_{2u}}}\frac{2M_d}{M_t}\delta_{\mu',\mu}. \quad \text{(C5)}$$

For the spin-conserving intervalley hole-phonon scattering in BL TMDs, with the intervalley hole-phonon scattering in each layer suppressed due to the large energy splitting,[1] holes in a given valley at a given layer are scattered into the other valley at different layer. Only the intervalley phonons, which induce the relative out-of-plane vibrations of the transition metal atoms in the two layers and hence lead to the variety of the interlayer hopping, can trigger this kind of the intervalley hole-phonon scattering. To derive the intervalley hole-phonon scattering matrix elements, one needs to know the intervalley phonon vibrations. As mentioned above, the BL phonon vibrations can be constructed by using the ML ones. Through the group theory analysis of ML lattice vibrations at the K point, which belongs to the space group C_{3h}, the decomposition into irreducible representations is as follows:

$${\rm K} = 2A'\oplus 2E'_1\oplus E'_2\oplus A''\oplus E''_1\oplus 2E''_2. \quad \text{(C6)}$$

Only the K_6 phonon modes[1] (correspond to the representation E''_2) are the out-of-plane vibrational modes, and

the vibrations of the two branches of K_6 phonons ($K_6^{\rm H}$ and $K_6^{\rm L}$) should be two kinds of orthogonal combinations of the out-of-plane vibration ψ_t of the transition metal atoms and the in-plane vibration ψ_d of the dichalcogenide atoms:

$$\psi_{K_6^{\rm L}} = \frac{\psi_d + A\psi_t}{\sqrt{M_{\rm W}+2A^2M_{\rm Se}}}, \tag{C7}$$

$$\psi_{K_6^{\rm H}} = \frac{A\sqrt{2M_{\rm Se}/M_{\rm W}}\psi_d - \sqrt{M_{\rm W}/2M_{\rm Se}}\psi_t}{\sqrt{M_{\rm W}+2A^2M_{\rm Se}}}. \tag{C8}$$

To obtain the specific combination A, one needs to solve the kinetic equation, which is beyond the scope of this investigation. We take $A=1$ approximately here.[77] Then, we construct BL intervalley phonon vibrations by using the ML ones in each layer but with opposite vibration directions between the two layers, and by using the tight-binding model according to the same work by Viljas and Heikkilä,[58] the scattering matrix elements are given by

$$|M^{K_6^{\rm L}}_{\mu\mu'\mathbf{q}}|^2 = \frac{t'^2_\perp}{2\rho\Omega_{K,K_6^{\rm L}}}\delta_{\mu',-\mu}, \tag{C9}$$

$$|M^{K_6^{\rm H}}_{\mu\mu'\mathbf{q}}|^2 = \frac{t'^2_\perp}{2\rho\Omega_{K,K_6^{\rm H}}}\frac{2M_d}{M_t}\delta_{\mu',-\mu}. \tag{C10}$$

Appendix D: Valley polarization from the KSBEs

With the hole density in each valley $N_\mu = {\rm Tr}(\rho_{\mu\mathbf{k}})$, by taking trace from both sides of the KSBEs, one obtains

$$\partial_t N_\mu = {\rm Tr}(\partial_t\rho_{\mu\mathbf{k}}|_{\rm coh}) + {\rm Tr}(\partial_t\rho_{\mu\mathbf{k}}|^{\rm intra}_{\rm scat}) + {\rm Tr}(\partial_t\rho_{\mu\mathbf{k}}|^{\rm inter}_{\rm scat}). \tag{D1}$$

Since the hole density in each valley is not affected by the spin precessions and intravalley scattering, one has ${\rm Tr}(\partial_t\rho_{\mu\mathbf{k}}|_{\rm coh}) = 0$ and ${\rm Tr}(\partial_t\rho_{\mu\mathbf{k}}|^{\rm intra}_{\rm scat}) = 0$. Additionally, in our calculation, the energy-splitting induced by the Zeeman-like term $\mu\eta E_z$ is much smaller than the Fermi energy, and hence by neglecting this energy splitting in Eq. (7), one has

$$\begin{aligned}\partial_t N_\mu = 2\pi\sum_{\mathbf{k}\mathbf{k}'\mathbf{q}\sigma\mu'}|M^\xi_{\mu\mu'}|^2\big\{&\big[f^\sigma_{\mu'\mathbf{k}+\mathbf{q}}(1-f^\sigma_{\mu\mathbf{k}})(N_\mathbf{q}+1) - f^\sigma_{\mu\mathbf{k}}(1-f^\sigma_{\mu'\mathbf{k}+\mathbf{q}})N_\mathbf{q}\big]\delta(\varepsilon_{\mathbf{k}+\mathbf{q}}-\varepsilon_\mathbf{k}-\Omega_\xi)\\ &+\big[f^\sigma_{\mu'\mathbf{k}+\mathbf{q}}(1-f^\sigma_{\mu\mathbf{k}})N_\mathbf{q} - f^\sigma_{\mu\mathbf{k}}(1-f^\sigma_{\mu'\mathbf{k}+\mathbf{q}})(N_\mathbf{q}+1)\big]\delta(\varepsilon_\mathbf{k}-\varepsilon_{\mathbf{k}+\mathbf{q}}-\Omega_\xi)\big\}.\end{aligned} \tag{D2}$$

As the hole distribution exhibits a quasi hot-hole Fermi distribution behavior [see the inset in Fig. 8(b)] in the temporal evolution, we use the hot-hole Fermi distribution characterized by $T_{\rm eff}$ in Eq. (D2). In addition, one has $N_\mathbf{q}\approx 0$ at low temperature ($k_BT \ll \Omega_\xi$), denoting the intervalley hole-phonon scattering through absorbing phonons is negligible. Therefore, with the larger density of spin-down (-up) holes in the K (K′) valley, Eq. (D2) in the degenerate limit becomes

$$\frac{\partial N_\mu}{\partial t} = \frac{\mu D_s}{2}\Big(\frac{\Delta E^\Uparrow}{\tau_{p\ \Uparrow}^{\rm K'\to K}} - \frac{\Delta E^\Downarrow}{\tau_{p\ \Downarrow}^{\rm K\to K'}}\Big), \tag{D3}$$

where

$$\tau_{p\ \Uparrow(\Downarrow)}^{\rm K'(K)\to K(K')} = \tau_p^*(e^{\beta_{\rm eff}^{\Uparrow(\Downarrow)}\Delta E^{\Uparrow(\Downarrow)}}-1), \tag{D4}$$

for $\Delta E^{\Uparrow(\Downarrow)} > 0$. The first (second) term on the right handside of Eq. (D3) comes from the contribution of the spin-conserving intervalley scattering of spin-up (-down) holes.

Substituting $N_{\rm K'} - N_{\rm K} = P_N N_h$ into Eq. (D4), the temporal evolution of the valley polarization reads

$$\frac{\partial P_N}{\partial t} = \frac{D_s}{N_h}\Big(\frac{\Delta E^\Downarrow}{\tau_{p\ \Downarrow}^{\rm K\to K'}} - \frac{\Delta E^\Uparrow}{\tau_{p\ \Uparrow}^{\rm K'\to K}}\Big). \tag{D5}$$

Next we derive Eq. (18) based on the KSBEs. Specifically, it has been shown that in the degenerate limit, the difference of the SRTs in the two valleys is suppressed by the intervalley hole-phonon scattering [see Fig. 8(b)]. With the contribution of the intravalley scatterings to the spin relaxation given in Eq. (B11), by neglecting the dephasing parts of the intervalley hole-phonon scattering since the intervalley hole-phonon scattering is in the weak-scattering limit, the temporal evolution of spin polarization in each valley becomes

$$\frac{\partial P_s^\mu}{\partial t} = -\frac{P_s^\mu}{\tau_{sz}^\mu} + \mu\frac{D_s}{N_h}\Big(\frac{\Delta E^\Downarrow}{\tau_{p\ \Downarrow}^{\rm K\to K'}} + \frac{\Delta E^\Uparrow}{\tau_{p\ \Uparrow}^{\rm K'\to K}}\Big). \tag{D6}$$

Further considering $\partial_t P_s^{\rm K} \approx \partial_t P_s^{\rm K'}$ in Eq. (D6), one has

$$\frac{2D_s}{N_h}\Big(\frac{\Delta E^\Downarrow}{\tau_{p\ \Downarrow}^{\rm K\to K}} + \frac{\Delta E^\Uparrow}{\tau_{p\ \Uparrow}^{\rm K'\to K}}\Big) \approx \frac{P_s^{\rm K}}{\tau_{sz}^{\rm K}} - \frac{P_s^{\rm K'}}{\tau_{sz}^{\rm K'}}. \tag{D7}$$

Additionally, $\partial_t P_N = 0$ in Eq. (D5) when the valley polarization reaches the maximum at $t = t_m$, and then by using Eqs. (D4) and (D7), one obtains

$$\frac{\Delta E^{\Uparrow(\Downarrow)}}{e^{\beta_{\rm eff}^{\Uparrow(\Downarrow)}\Delta E^{\Uparrow(\Downarrow)}}-1} = \frac{\tau_p^* N_h}{4D_s}\left(\frac{P_s^{\rm K}}{\tau_{sz}^{\rm K}} - \frac{P_s^{\rm K'}}{\tau_{sz}^{\rm K'}}\right). \qquad \text{(D8)}$$

Taking $\beta_{\rm eff}^{\Downarrow(\Uparrow)}\Delta E_F^{\Downarrow(\Uparrow)} \ll 1$ and $P_N N_h = D_s(\Delta E_F^{\Uparrow} - \Delta E_F^{\Downarrow})$, the maximum of the valley polarization [Eq. (18)] is obtained.

* Author to whom correspondence should be addressed; Electronic address: mwwu@ustc.edu.cn.

[1] Y. Song and H. Dery, Phys. Rev. Lett. **111**, 026601 (2013).
[2] H. Ochoa and R. Roldan, Phys. Rev. B **87**, 245121 (2013).
[3] H. Ochoa, F. Guinea, and V. I. Fal'ko, Phys. Rev. B **88**, 195417 (2013).
[4] L. Wang and M. W. Wu, Phys. Lett. A **378**, 1336 (2014).
[5] L. Wang and M. W. Wu, Phys. Rev. B **89**, 115302 (2014).
[6] S. D. Conte, F. Bottegoni, E. A. A. Pogna, S. Ambrogio, I. Bargigia, C. D'Andrea, D. D. Fazio, A. Lombardo, M. Bruna, F. Ciccacci, A. C. Ferrari, G. Cerullo, and M. Finazzi, arXiv:1502.06817.
[7] T. Y. Yan, X. F. Qiao, P. H. Tan, and X. H. Zhang, arXiv:1502.07088.
[8] A. Splendiani, L. Sun, Y. Zhang, T. Li, J. Kim, C. Y. Chim, G. Galli, and F. Wang, Nano Lett. **10**, 1271 (2010).
[9] K. F. Mak, C. Lee, J. Hone, J. Shan, and T. F. Heinz, Phys. Rev. Lett. **105**, 136805 (2010).
[10] G. Eda, H. Yamaguchi, D. Voiry, T. Fujita, M. Chen, and M. Chhowalla, Nano Lett. **11**, 5111 (2011).
[11] Z. Y. Zhu, Y. C. Cheng, and U. Schwingenschlögl, Phys. Rev. B **84**, 153402 (2011).
[12] D. Xiao, G.-B. Liu, W. Feng, X. Xu, and W. Yao, Phys. Rev. Lett. **108**, 196802 (2012).
[13] E. S. Kadantsev and P. Hawrylak, Solid State Commun. **152**, 909 (2012).
[14] K. Kaasbjerg, K. S. Thygesen, and K. W. Jacobsen, Phys. Rev. B **85**, 115317 (2012).
[15] T. Cheiwchanchamnangij and W. R. L. Lambrecht, Phys. Rev. B **85**, 205302 (2012).
[16] K. Kośmider and J. F. Rossier, Phys. Rev. B **87**, 075451 (2013).
[17] F. Zahid, L. Liu, Y. Zhu, J. Wang, and H. Guo, AIP Advances **3**, 052111 (2013).
[18] H. Shi, H. Pan, Y. W. Zhang, and B. I. Yakobson, Phys. Rev. B **87**, 155304 (2013).
[19] W. Yao, D. Xiao, and Q. Niu, Phys. Rev. B **77**, 235406 (2008).
[20] T. Cao, G. Wang, W. Han, H. Ye, C. Zhu, J. Shi, Q. Niu, P. Tan, E. Wang, B. Liu, and J. Feng, Nat. Commun. **3**, 887 (2012).
[21] G. Sallen, L. Bouet, X. Marie, G. Wang, C. R. Zhu, W. P. Han, Y. Lu, P. H. Tan, T. Amand, B. L. Liu, and B. Urbaszek, Phys. Rev. B **86**, 081301 (2012).
[22] D. Lagarde, L. Bouet, X. Marie, C. R. Zhu, B. L. Liu, T. Amand, P. H. Tan, and B. Urbaszek, Phys. Rev. Lett. **112**, 047401 (2014).
[23] H. L. Zeng, J. F. Dai, W. Yao, D. Xiao, X. D. Cui, Nat. Nanotechnol. **7**, 490 (2012).
[24] K. F. Mak, K. L. He, J. Shan, T. F. Heinz, Nat. Nanotechnol, **7**, 494 (2012).
[25] C. Mai, A. Barrette, Y. F. Yu, Y. G. Semenov, K. W. Kim, L. Y. Cao, and K. Gundogdu, Nano Lett. **14**, 202 (2014).
[26] Y. L. Li, J. Ludwig, T. Low, A. Chernikov, X. Cui, G. Arefe, Y. D. Kim, A. M. V. D. Zande, A. Rigosi, H. M. Hill, S. H. Kim, J. Hone, Z. Q. Li, D. Smirnov, T. F. Heinz, Phys. Rev. Lett. **113**, 266804 (2014).
[27] G. Aivazian, Z. R. Gong, A. M. Jones, R. L. Chu, J. Yan, D. G. Mandrus, C. W. Zhang, D. Cobden, W. Yao, X. Xu, Nat. Phys. **11**, 148 (2015).
[28] Y. Yafet, Phys. Rev. **85**, 478 (1952).
[29] R. J. Elliott, Phys. Rev. **96**, 266 (1954).
[30] M. I. D'yakonov and V. I. Perel', Zh. Eksp. Teor. Fiz. **60**, 1954 (1971) [Sov. Phys. JETP **33**, 1053 (1971)].
[31] A. Ramasubramanlam, D. Naveh, and E. Towe, Phys. Rev. B **84**, 205325 (2011).
[32] S. F. Wu, J. S. Ross, G. B. Liu, G. Aivazian, A. Jones, Z. Y. Fei, W. G. Zhu, D. Xiao, W. Yao, D. Cobden, and X. D. Xu, Nat. Phys. **9**, 149 (2013).
[33] H. T. Yuan, M. S. Bahramy, K. Morimoto, S. F. Wu, K. Nomura, B. J. Yang, H. Shimotani, R. Suzuki, M. Toh, C. Kloc, X. D. Xu, R. Arita, N. Nagaosa, and Y. Iwasa, Nat. Phys. **9**, 563 (2013).
[34] E. Cappelluti, R. Roldán, J. A. S. Guillén, P. Ordejón, and F. Guinea, Phys. Rev. B **88**, 075409 (2013).
[35] Z. R. Gong, G. B. Liu, H. Yu, D. Xiao, X. D. Cui, X. D. Xu, and W. Yao, Nat. Commu. **4**, 2053 (2013).
[36] A. M. Jones, H. Yu, J. S. Ross, P. Klement, N. J. Ghimire, J. Q. Yan, D. G. Mandrus, W. Yao, and X. D. Xu, Nat. Phys. **10**, 130 (2014).
[37] S. B. Desai, G. Seol, J. S. Kang, H. Fang, C. Battaglia, R. Kapadia, J. W. Ager, J. Guo, and A. Javey, Nano. Lett. **14**, 4592 (2014).
[38] B. R. Zhu, H. L. Zeng, J. F. Dai, Z. R. Gong, and X. D. Cui, Proc. Natl. Acad. Sci. **111**, 11607 (2014).
[39] T. Yu and M. W. Wu, Phys. Rev. B **90**, 035437 (2014).
[40] H. Sahin, S. Tongay, S. Horzum, W. Fan, J. Zhou, J. Li, J. Wu, and F. M. Peeters, Phys. Rev. B **87**, 165409 (2014).
[41] X. D. Xu, W. Yao, D. Xiao, T. F. Heinz, Nat. Phys. **10**, 343 (2014).
[42] R. Roldán, M. P. L. Sancho, F. Guinea, E. Cappelluti, J. A. S. Guillén, and P. Ordejón, 2D Matter. **1**, 034003 (2014).
[43] L. Debbichi, O. Erlksson, and S. Lebégue, Phys. Rev. B **89**, 205311 (2014).
[44] B. Zhu, X. Chen, and X. D. Cui, Sci. Rep. **5**, 9218 (2015).
[45] C. Y. Wang and G. Y. Guo, J. Phys. Chem. C **10**, 1021 (2015).
[46] D. H. Li, R. Cheng, H. L. Zhou, C. Wang, A. X. Yin, Y. Chen, N. O. Weiss, Y. Huang, and X. F. Duan, arXiv:1501.02422.
[47] M. Q. Weng and M. W. Wu, Phys. Rev. B **68**, 075312 (2003).
[48] M. W. Wu, J. H. Jiang and M. Q. Weng, Phys. Rep. **493**, 61 (2010).
[49] T. Yu and M. W. Wu, Phys. Rev. B **89**, 045303 (2014).

[50] D. Stich, J. Zhou, T. Korn, R. Schulz, D. Schuh, W. Wegscheider, M. W. Wu, and C. Schüller, Phys. Rev. Lett. **98**, 176401 (2007); Phys. Rev. B **76**, 205301 (2007).

[51] *Optical Orientation*, edited by F. Meier and B. P. Zakharchenya (North-Holland, 1984).

[52] T. Yu and M. W. Wu, Phys. Rev. B **89**, 205303 (2014).

[53] A. Kormányos, V. Zólyomi, N. D. Drummond, and G. Burkard, Phys. Rev. X **4**, 011034 (2014).

[54] P. O. Löwdin, J. Chem. Phys. **19**, 1396 (1951).

[55] R. Winkler, *Spin-orbit Coupling Effect in Two-Dimensional Electron and hole Systems* (Springer, Berlin, 2003).

[56] J. Zhou, J. L. Cheng, and M. W. Wu, Phys. Rev. B **75**, 045305 (2007).

[57] Y. Zhou and M. W. Wu, Phys. Rev. B **82**, 085304 (2010).

[58] J. K. Viljas and T. T. Heikkilä, arXiv:1002.3502.

[59] Z. H. Jin, X. D. Li, J. T. Mullen, and K. W. Kim, Phys. Rev. B **90**, 045422 (2014). [It is noted that the leading terms of the deformation potentials of the intervalley electron-phonon scatterings (including $D_{\mathbf{K},\mathrm{TA/LA}}$ and $D_{\mathbf{K},\mathrm{TO}}$) in this paper are in zeroth-order, differing from the work by Kassbjerg *et al.*[78] where the leading contributions of the corresponding terms are in first-order.]

[60] J. L. Verble and T. J. Wieting, Phys. Rev. Lett. **25**, 362 (1970).

[61] X. Zhang, W. P. Han, J. B. Wu, S. Milana, Y. Lu, Q. Q. Li, A. C. Ferrari, and P. H. Tan, Phys. Rev. B **87**, 115413 (2013).

[62] Y. Y. Zhao, X. Luo, H. Li, J. Zhang, P. T. Araujo, C. K. Gan, J. Wu, H. Zhang, S. Y. Quek, M. S. Dresselhaus, and Q. H. Xiong, Nano Lett. **13**, 1007 (2013).

[63] H. Terrones, E. D. Corro, S. Feng, J. M. Poumirol, D. Rhodes, D. Smirnov, N. R. Pradhan, Z. Lin, M. A. T. Nguyen, A. L. Elias, T. E. Mallouk, L. Balicas, M. A. Pimenta, M. Terrones, Sci. Rep. **4**, 4215 (2014).

[64] V. Podzorov and M. E. Gershenson, Appl. Phys. Lett. **84**, 1726 (2004).

[65] H. Fang, S. Chuang, T. C. Chang, K. Takei, T. Takahashi, and A. Javey, Nano Lett. **12**, 3788 (2012).

[66] A. Allain and A. Kis, ACS Nano **8**, 7180 (2014).

[67] X. Z. Ruan, H. H. Luo, Y. Ji, Z. Y. Xu, and V. Umansky, Phys. Rev. B **77**, 193307 (2008).

[68] J. H. Jiang and M. W. Wu, Phys. Rev. B **79**, 125206 (2009).

[69] M. M. Glazov and E. L. Ivchenko, Zh. Eksp. Teor. Fiz. **126**, 1465 (2004) [JEPT **99**, 1279 (2004)].

[70] G. F. Giuliani and G. Vignale, *Quantum Theory of the Electron Liquid* (Cambridge University Press, Cambridge, England, 2005).

[71] P. Zhang and M. W. Wu, Phys. Rev. B **80**, 155311 (2009).

[72] B. Y. Sun, P. Zhang, and M. W. Wu, J. Appl. Phys. **108**, 093709 (2009).

[73] L. F. Han, Y. G. Zhu, X. H. Zhang, P. H. Tan, H. Q. Ni, and Z. C. Niu, Nanoscale Res. Lett. **6**, 84 (2011).

[74] P. Zhang, Y. Zhou, and M. W. Wu, J. Appl. Phys. **112**, 073709 (2012).

[75] N. Zibouche, P. Philipsen, A. Kue, and T. Heine, Phys. Rev. B **90**, 125440 (2014).

[76] N. Zibouche, P. Philipsen, T. Heine, and A. Kue, Phys. Chem. Chem. Phys. **16**, 11251 (2014).

[77] M. Tinkham, *Group Theory and Quantum Mechanics* (McGraw-Hill Book Company, Inc., 1964).

[78] K. Kassbjerg, K. S. Bhargavi, and S. S. Kubakaddi, Phys. Rev. B **90**, 165436 (2014).